Geochimica et Cosmochimica Acta 372 (2024) 134–153

Contents lists available at ScienceDirect

Geochimica et Cosmochimica Acta

journal homepage: www.elsevier.com/locate/gca

Refining the roles of productivity, redox, and remineralization on the cadmium isotope composition of marine sediments

Logan A. Tegler [a,b,c,*], Sune G. Nielsen [a,d,1], Yi Wang [a,d,2], Florian Scholz [e,3], Jeremy D. Owens [f], Larry Peterson [g], Maureen Auro [a,b], Christopher W. Kinsley [a,c,4], Phoebe Lam [h], Tristan J. Horner [a,b]

[a] NIRVANA Laboratories, Woods Hole Oceanographic Institution, Woods Hole, MA 02543, United States
[b] Department of Marine Chemistry and Geochemistry, Woods Hole Oceanographic Institution, Woods Hole, MA 02543, United States
[c] Department of Earth, Atmospheric and Planetary Sciences, Massachusetts Institute of Technology, Cambridge, MA 02139, United States
[d] Department of Marine Geology and Geophysics, Woods Hole Oceanographic Institution, Woods Hole, MA 02543, United States
[e] GEOMAR Helmholtz Centre for Ocean Research Kiel, Kiel, Germany
[f] Department of Earth, Ocean and Atmospheric Science, Florida State University and National High Magnetic Field Laboratory, Tallahassee, FL, United States
[g] Department of Marine Geosciences, Rosenstiel School of Marine, Atmospheric, and Earth Science, University of Miami, Miami, FL, United States
[h] Department of Ocean Sciences, University of California Santa Cruz, Santa Cruz, CA, 95064, United State

ARTICLE INFO

Associate editor: Susan Halsall Little

Keywords:
CdS precipitation
Continental margin
Paleo-proxy
Isotope fractionation
Marine particulate matter

ABSTRACT

Cadmium (Cd) has a nutrient-like distribution in the ocean, similar to the macronutrient phosphate. Significant isotope fractionation induced by the biological cycling of Cd makes it a potential tracer for nutrients and productivity. However, the Cd flux and Cd isotope composition of marine sediments may also be influenced by local redox conditions and partial remineralization of organically hosted Cd. These confounding factors are underconstrained and render it challenging to use Cd as a reliable paleoproxy. To understand the relative importance of each of these processes, we examined the Cd isotope systematics of 69 modern sediments deposited across a wide range of environments. We complement these data with four profiles of particulate Cd isotope compositions from the Southern Ocean. We report three main results. First, we show that the sedimentary flux of Cd is tightly coupled to that of organic matter. Second, most Cd burial occurs in regions with some bottom-water oxygen, and the flux of CdS to anoxic regions is, globally, minor. Finally, we find that remineralization can substantially modify sedimentary Cd isotope compositions, though it is challenging to relate pelagic and sedimentary processes. For example, we find that the relationship between sedimentary Cd isotope compositions and surface seawater [Cd] is the reverse of that predicted by isotope reactor models. Likewise, sedimentary Cd isotope compositions are anti-correlated with bottom-water oxygen. While this pattern is consistent with preferential remineralization of isotopically heavy Cd, profiles of marine particulate matter reveal the reverse, whereby the Cd isotope composition of large particles, which are most likely to reach the seafloor, becomes increasingly 'heavy' with depth. These results highlight how productivity, redox, and remineralization all influence the flux and isotope composition of Cd to marine sediments. While our study suggests that there is no simple way to relate sedimentary Cd isotopes to surface nutrient utilization, our data point toward several potential controls that could form the basis of novel proxies for local redox conditions and remineralization.

* Corresponding author at: Department of Oceanography, School of Ocean and Earth Science and Technology, University of Hawai'i at Mānoa, Honolulu, HI, USA.
E-mail addresses: tegler@hawaii.edu (L.A. Tegler), snielsen@whoi.edu (S.G. Nielsen), ywang145@tulane.edu (Y. Wang), florian.scholz@uni-hamburg.de (F. Scholz), jdowens@fsu.edu (J.D. Owens), lpeterson@miami.edu (L. Peterson), mauro@whoi.edu (M. Auro), ckinsley@bgc.org (C.W. Kinsley), pjlam@ucsc.edu (P. Lam), tristan.horner@whoi.edu (T.J. Horner).
[1] Now at: CRPG, CNRS, Université de Lorraine, 15 rue Notre Dame des Pauvres, 54501 Vandoeuvre lès Nancy, France.
[2] Now at: Department of Earth and Environmental Sciences, Tulane University, New Orleans, 70118, United State.
[3] Now at: Institute for Geology, Center for Earth System Research and Sustainability, Universität Hamburg, Hamburg, Germany.
[4] Berkeley Geochronology Center, Berkeley, CA 94709.

https://doi.org/10.1016/j.gca.2024.03.010
Received 28 July 2023; Accepted 11 March 2024
Available online 18 March 2024

1. Introduction

Cadmium (Cd) displays a nutrient-like profile in the ocean with a distribution similar to the macronutrient phosphate (Boyle et al., 1976; Bruland, 1980). Despite its nutrient-like behavior, there is considerable debate about whether Cd serves an important physiological function (Lane et al., 2005) or is simply mistakenly incorporated by microbes as they search for other biologically essential metals (Boyle et al., 1988; Horner et al., 2013). Regardless of cadmium's biological function, Cd is intensely cycled by microbes in the upper water column (Sunda, 2012) and its relationship with P underpins its use as a proxy for nutrients and circulation (Boyle, 1988; Marchitto and Broecker, 2006).

Biological uptake of Cd is generally accompanied by a significant negative Cd isotopic fractionation, which can be traced throughout the water column. Studies have shown that phytoplankton preferentially take up the light isotope (Lacan et al., 2006; John and Conway, 2014), leaving the residual seawater heavier by up to $\delta^{114}Cd = +5$ ‰ relative to deep waters, (where $\delta^{114}Cd = {}^{114}Cd/{}^{110}Cd_{sample} / {}^{114}Cd/{}^{110}Cd_{NIST\ SRM\ 3108} - 1$). In contrast, the deep and intermediate ocean are nearly homogeneous with respect to $\delta^{114}Cd$, exhibiting values between + 0.25 and + 0.45 ‰ (Ripperger et al., 2007; Abouchami et al., 2014; Conway and John, 2015b; Sieber et al., 2023). The isotope composition of Cd in surface waters can theoretically provide information about the relative degree of nutrient utilization in a region, akin to carbon, nitrogen, or silicon isotopes (Farmer et al., 2021; Horner et al., 2021). In general, heavier Cd isotope compositions in surface seawater imply a higher level of local nutrient utilization, whereas lighter Cd isotope compositions indicate the reverse. However, studies have shown that this relationship breaks down at very low surface Cd concentrations; small additions of Cd – either from upward mixing of deep Cd (Abouchami et al., 2011; Xue et al., 2013) or downward deposition of anthropogenic aerosols and dust particles (Yang et al., 2012; Bridgestock et al., 2017; Sieber et al., 2023) – may obfuscate the biological $\delta^{114}Cd$ signal. However, little work has been done to investigate the relationship between surface water nutrient utilization and Cd isotope compositions recorded in marine sediments, which is a prerequisite for using Cd isotopes as a proxy for nutrient utilization (Georgiev et al., 2015).

Nearly all modern Cd burial is associated with organic matter-rich sediments (van Geen et al., 1995; Morford and Emerson, 1999; Little et al., 2015). While there are some minor sedimentary sinks of Cd, including burial with marine carbonates (Boyle, 1988; Horner et al., 2011) and removal with Fe-Mn sediments (Schmitt et al., 2009; Horner et al., 2010), >90 % of Cd is burial occurs into organic-rich sediments deposited along continental margins (Rosenthal et al., 1995a; van Geen et al., 1995; Little et al., 2015). Margins account for most global organic matter deposition and have enhanced Cd concentrations relative to the detrital background of Cd (i.e., 0.1 μg/g; van Geen et al., 1995). While much of the Cd that is deposited along margins is supported by Cd incorporation into organic matter, some Cd in the sediment occurs in excess of this value and is likely associated with Cd sulfides.

Cadmium sulfide formation has been predicted to occur through three primary pathways. First, some studies have posited that an abiotic mechanism may allow CdS to form within sulfidic microenvironments of sinking particles (Janssen et al., 2014; Conway and John, 2015a). However, several recent studies have suggested that this mechanism is not significant; instead, these studies suggest that the observed dissolved Cd deficiency in the water column may arise through biotic (e.g., Ohnemus et al., 2017) or physical processes, perhaps related to lower $Cd:PO_4$ in intermediate waters relative to deep waters (Ohnemus et al., 2017; de Souza et al., 2022; Sieber et al., 2023). Given the contentious nature of this supposed Cd sink, and the difficulty in distinguishing it from other forms of CdS, we do not consider CdS formation within sinking particles in our study. Second, CdS formation may occur pelagically in bottom water, particularly in low-oxygen, or anoxic (no detectable oxygen) environments. A recent study indicated that cadmium sulfide minerals could be precipitated directly from seawater in the presence of even trace amounts of dissolved H_2S (Plass et al., 2020). Third, when Cd bound in organic matter is delivered to the seafloor, organic matter can be remineralized within the sediment. If the Cd that was formerly bound in organic matter is liberated into porewaters that contain even trace levels dissolved H_2S, Cd can be recaptured into cadmium sulfide minerals (Gobeil et al., 1987; McCorkle and Klinkhammer, 1991). Indeed, previous work suggests that most authigenic Cd hosted in sediments is present as CdS (Rosenthal et al., 1995a; 1995b; van Geen et al., 1995).

The precipitation of Cd into sulfides is associated with a slight negative isotope fractionation (Guinoiseau et al., 2018). Thus, CdS formation in the environment has the potential to render changes in the Cd isotope composition of marine sediments. If, however, the capture of Cd is quantitative, the Cd isotope composition of sediments would reflect the source—bottom seawater or organic matter. The latter is noteworthy because it suggests that sediments may retain the Cd isotope composition of exported organic matter, even if the organic matter itself is no longer present. It is probable that CdS precipitation quantitatively consumes ambient Cd within the sediment. Even in cases where H_2S concentrations in the porewater are undetectable, CdS precipitation is nonetheless expected due to the extremely low stoichiometric solubility product of CdS, rendering CdS precipitation thermodynamically favorable (Rosenthal et al., 1995a). On the other hand, quantitative precipitation is not expected for Cd precipitation that occurs in seawater. Unfortunately, the relative importance of each of these CdS fluxes compared to organically bound fluxes are not well constrained. Isotope analysis may be able to help tease these sources of CdS apart.

Recent studies indicate that continental margin sediments unaffected by pelagic CdS precipitation from seawater exhibit Cd isotope compositions lighter than of deep water (Bryan et al., 2021; Chen et al., 2021). This finding is in line with the expectation that the global mass flux sink of $\delta^{114}Cd$ should broadly reflect the input value of dust and rivers, between +0.1 and +0.2 ‰ (Lambelet et al., 2013; Bridgestock et al., 2017). Likewise, it is consistent with a potential relationship between Cd isotopes and nutrient utilization that could be used as a paleonutrient proxy (Georgiev et al., 2015; Hohl et al., 2019). However, a recent study showed that suspended particulate matter in the North Pacific Ocean had isotope compositions that were far lighter than expected based on surface isotope values (Janssen et al., 2019). The authors of that study attributed the light isotope signature to a few possible processes, including remineralization, which may alter the Cd isotope composition of the primary particles. If this process affects the particles that eventually settle on the seafloor, it will affect the isotope composition of sedimentary Cd isotopes, but this process has not been explored. Such a study is important to evaluate the potential of sedimentary Cd isotopes as a paleo nutrient proxy.

Here, we explore the roles of redox, productivity, and remineralization in shaping the Cd isotope compositions of recent organic-rich sediments. We specifically aimed to answer three questions: (i) Can we differentiate between regions that have substantial CdS formation from those that do not using Cd isotopes and concentrations in the sediment? (ii) Is there a way to relate the Cd isotope composition of sinking or suspended particulate matter to what we observe on the seafloor? And, (iii) Do regions that are dominated by Cd derived from organic matter record nutrient utilization from in overlying the surface waters? To answer these questions, we examine sediments deposited under various bottom-water redox conditions, consider these data alongside data for sediments from the California margin, and report Cd isotope data for particulate organic matter from the Ross Sea. Our dataset suggests that ambient redox conditions, remineralization, and external Cd additions may all influence the Cd isotope composition of the underlying sediment.

2. Samples, sampling, and site description

2.1. Sediment samples and regional settings

Sixty-nine sediment samples were selected across the globe to cover a range of redox conditions (Fig. 1, Table 1). The sediments in this study span a redox gradient from euxinic (anoxic and sulfidic waters, e.g., Black Sea and Cariaco Basin), anoxic (e.g., Cariaco Basin and Peru Upwelling Region), and oxic (e.g., Peru Upwelling, Santa Barbara Basin, Western Equatorial Pacific, Arabian Sea, and Namibian Margin) bottom water conditions. The samples will be briefly described here.

The 12 Black Sea sediment samples were collected on the R/V *Knorr* Cruise 134 Leg 8 in 1988. The Black Sea is the modern ocean's largest euxinic basin. The basin is defined by a constant halocline that restricts vertical mixing below 60–80 m (Yakushev et al., 2010). Beneath the halocline, oxygen is depleted as it is used for microbial respiration. Subsequent anoxic respiration creates persistent hydrogen sulfide in the water column (Konovalov and Murray, 2001; Konovalov et al., 2001). The Black Sea has only limited exchange with open ocean seawater as it is an intracontinental basin. Thus, the Black Sea is likely to be heavily influenced by changes in riverine input. The subsamples collected were stored frozen in the Woods Hole Oceanographic (WHOI) Seafloor Samples Laboratory. Five of these are down core samples (i.e., non-coretop) taken from Station 39 box core 21 below the chemocline at a water depth of 2,092 m. These samples were described in detail elsewhere (Arthur et al., 1994; Owens et al., 2017). The box core samples recovered were a Holocene finely laminated sapropel (0–25 cm; Owens et al., 2017). The remaining seven sub-samples, also collected from the core repository, were taken at various water depths between 184 and 2,215 m. The sample depths (i.e., core-top, or down core) for each of the samples are given in Table 1.

Cariaco Basin sediments were collected on the 1990 PLUME Cruise Leg 7 (R/V *Thomas Washington*). The Cariaco Basin is a large euxinic basin off the coast of Venezuela that spans about 7,000 km^2 (Peterson et al., 1990). The basin is restricted from the Caribbean Sea by shallow sills to the west (146 m) and north (120 m; Fig. 1). There is high productivity in the region from seasonal upwelling along the coast, which, coupled with significant microbial respiration and lack of deep-water renewal, leads to the depletion of oxygen and the increase of hydrogen sulfide in the water. Thus, the basin water becomes euxinic at a water depth of ≈300 m. Additional information on the seawater and sediments can be found in (Astor et al., 2011) and (Peterson et al., 1990), respectively. The samples measured in this study were box core top samples and were collected below the permanent chemocline (400 to 1,400 m). These sediments were made up of fine-grained clay with various carbonate and calcareous ooze (Wu et al., 2020).

Peruvian Margin samples were collected along 11°S in 2008 on the M77-1 Cruise (R/V *Meteor*). The Peru Margin is defined by offshore Ekman transport off the coast of South America that creates coastal upwelling of nutrient-rich and oxygen-depleted water supplied by the Peru-Chile Undercurrent. The upwelling of nutrient-rich and oxygen-depleted waters leads to high levels of primary productivity in the region. The elevated levels of primary productivity are linked to high demands for oxygen during oxic microbial respiration (Pennington et al., 2006). Thus, the region is characterized by a perennial oxygen minimum zone (OMZ) off the coast of the Peruvian shelf between approximately 50 and 500 m (Suess and Huene, 1988; Scholz et al., 2011). During periods of water stagnation, the water column can become anoxic and depleted in both nitrate and nitrite following denitrification (Sommer et al., 2016). When this depletion occurs, hydrogen

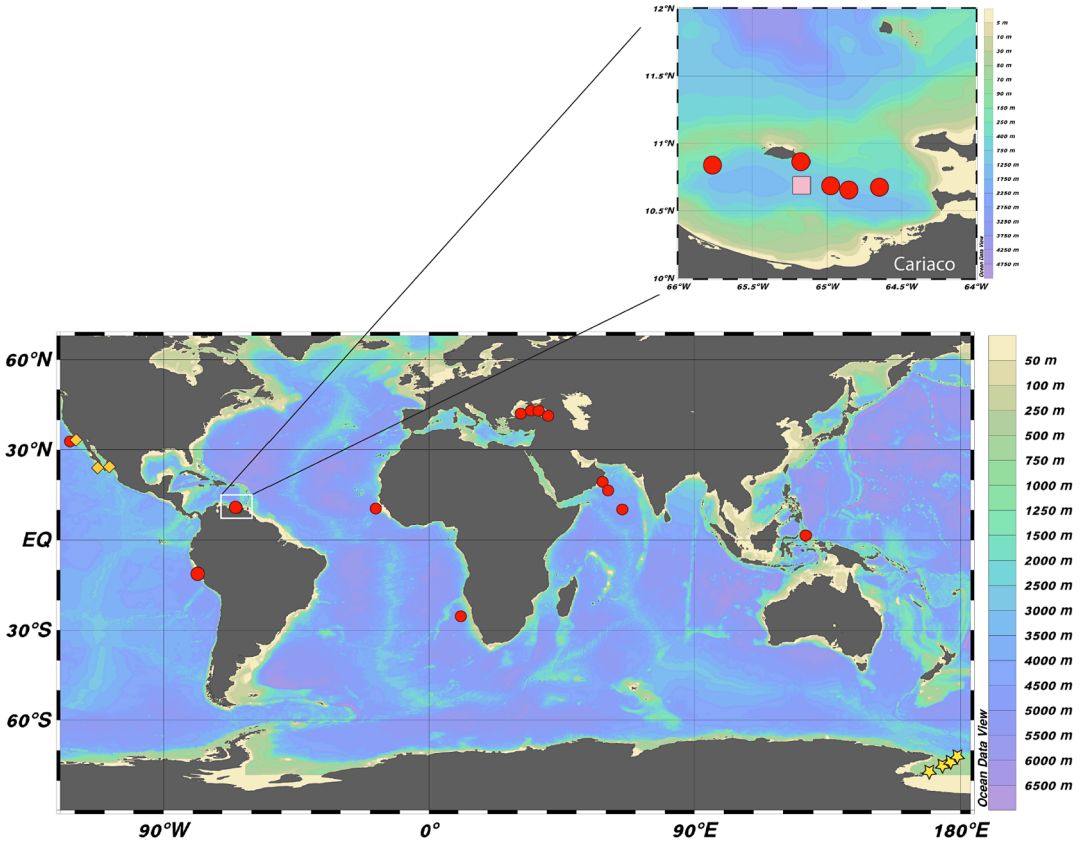

Fig. 1. Map showing sample locations. Circles indicate locations of the sites studied along the continental margins. Individual sample locations within a region are not always plotted due to close proximity to other samples within that region. Diamonds are locations of samples in the northeastern Pacific margin from Chen et al. (2021). Square denotes samples from the Cariaco Basin from Little et al. (2015). Stars denote samples from the Ross Sea. Maps were made using Ocean Data View (odv.awi.de; Schlitzer, 2017).

Table 1
Summary of sedimentary results, including sample information and leached Cd concentrations and isotopes.

Location	Sample Name	Latitude (deg)	Longitude (deg)	Top depth in sediment (cm)	Bottom depth in sediment (cm)	Coring Water Dept (m)	Bottom Water O2 (μM)	O_2 estimate	OC (%)	Cd (μg/g)	δ^{114}Cd (‰)	2SD (‰)	$[Cd]_{surf}$ (nM)	Reference
Arabian Sea	TOM41 MC32C	19.50	58.47	0	1	611	1	WOA18	1.81	1.89	0.15	0.03	0.080	This study
Arabian Sea	TOM41-17E	15.99	61.53	2	3	3985	129	WOA18	0.57	0.22	−0.05	0.03	0.011	This study
Arabian Sea	TOM41-32G	19.50	58.47	0	1	611	1	WOA18	2.17	1.52	0.09	0.03	0.080	This study
Arabian Sea	TOM41-MC17A	15.99	61.53	2	3	3985	129	WOA18	0.53	0.23	−0.05	0.03	0.011	This study
Arabian Sea	TOM41-MC22E	10.03	65.08	2	3	4426	160	WOA18	0.33	0.11	−0.12	0.03	0.004	This study
Arabian Sea	TOM41-MC29G	17.20	59.95	3	4	2431	107	WOA18	0.59	0.11	0.00	0.03	0.013	This study
Arabian Sea	TOM47 26F	19.21	58.27	1	2	513	3	WOA18	1.51	0.41	0.15	0.03	0.071	This study
Arabian Sea	TOM47 MC26D	19.21	58.27	3	4	513	3	WOA18	2.43	0.96	0.09	0.03	0.071	This study
Arabian Sea	TOM47 MC30H	19.22	58.02	5	6	71	6	WOA18	0.57	0.44	0.25	0.03	0.075	This study
Arabian Sea	TOM47 MC34D	19.52	58.49	5	6	719	6	WOA18	5.94	2.22	0.09	0.03	0.080	This study
Black Sea	BS1-2CM	43.09	32.03	1	2	2092	0	Measured	6.00	0.62	0.12	0.03	0.820	This study
Black Sea	BS2-3CM	43.09	32.03	2	3	2092	0	Measured	6.00	1.14	0.03	0.04	0.820	This study
Black Sea	BS3-4CM	43.09	32.03	3	4	2092	0	Measured	6.00	1.06	0.18	0.03	0.820	This study
Black Sea	BS30-31CM	43.09	32.03	30	31	2092	0	Measured	6.00	0.22	0.19	0.03	0.820	This study
Black Sea	BS48-49CM	43.09	32.03	48	49	2092	0	Measured	6.00	1.68	0.18	0.03	0.820	This study
Black Sea	BSBC47	41.45	40.36	0	1	184	0	WOA18	0.93	0.35	−0.01	0.03	0.792	This study
Black Sea	BSBC84	42.37	31.89	0	1	2212	0	WOA18	1.24	0.20	0.09	0.03	0.800	This study
Black Sea	BSGGC14	41.79	30.48	11	12	1916	1	WOA18	1.18	0.17	0.04	0.03	0.762	This study
Black Sea	BSGGC16	42.43	30.65	6	7	2170	0	WOA18	1.01	0.14	0.02	0.03	0.820	This study
Black Sea	BSGGC68	42.99	34.01	0	1	2221	0	WOA18	4.20	0.60	0.19	0.03	0.806	This study
Black Sea	BSWHGGC-80	42.51	33.22	0	1	2215	1	WOA18	2.23	0.34	0.11	0.03	0.795	This study
Black Sea	BSWHGGC32	43.10	36.60	21	22	2186	0	WOA18	2.87	0.46	0.12	0.04	0.831	This study
Cariaco Basin	CB111BC	10.84	−65.78	0	1	411	0	Measured	3.26	1.43	0.28	0.03	0.014	This study
Cariaco Basin	CB22BC	10.87	−65.17	0	1	656	0	Measured	5.27	2.27	0.26	0.03	0.007	This study
Cariaco Basin	CB67BC	10.69	−64.66	0	1	400	0	Measured	5.57	1.72	0.27	0.03	0.007	This study
Cariaco Basin	CB82BC	10.66	−64.86	0	1	1342	0	Measured	5.95	1.76	0.25	0.03	0.010	This study
Cariaco Basin	CB89BC	10.69	−64.97	0	1	818	0	Measured	5.19	1.76	0.34	0.03	0.010	This Study
Namibian Margin	CHN115- 17PH	−25.01	10.67	0	1	4254	218	WOA18	0.17	0.84	−0.18	0.03	0.042	This study
Namibian Margin	CHN99 8 PG	10.51	−18.31	2	5	4014	242	WOA18	0.73	1.17	−0.15	0.03	0.006	This study
Peru Margin	PM-Stn481-30–34	−11.00	−78.24	30	34	376	2	Measured	3.34	15.81	0.24	0.03	0.194	This study
Peru Margin	PM-Stn449-14–18	−11.00	−78.17	14	18	319	2	Measured	13.45	16.73	0.13	0.03	0.246	This study
Peru Margin	PM-Stn549-7	−11.00	−78.52	7	7	1005	42	Measured	3.33	0.86	0.12	0.03	0.152	This study
Peru Margin	PM-Stn449-8–10	−11.00	−78.17	8	10	319	2	Measured	16.17	32.25	0.22	0.03	0.246	This study
Peru Margin	PM-Stn568-10	−11.00	−77.80	10	10	85	2	Measured	2.31	15.53	0.31	0.03	0.326	This study
Peru Margin	PM-Stn462-14	−11.00	−78.75	14	14	2025	93	Measured	2.09	1.09	0.13	0.03	0.137	This study
Peru Margin	PM-Stn568-14	−11.00	−77.80	14	14	85	2	Measured	3.28	16.90	0.34	0.03	0.326	This study
Peru Margin	PM-Stn470-18–22	−11.00	−77.94	18	22	145	2	Measured	7.13	50.80	0.31	0.03	0.294	This study
Peru Margin	PM-Stn459-22–26	−11.00	−78.43	22	26	697	13	Measured	5.62	3.85	0.08	0.03	0.162	This study
Peru Margin	PM-Stn470-22–26	−11.00	−77.94	22	26	145	2	Measured	7.46	48.97	0.25	0.03	0.294	This study
Peru Margin	PM-Stn481-22–26	−11.00	−78.24	22	26	376	2	Measured	12.02	14.49	0.15	0.03	0.194	This study
Peru Margin	PM-Stn449-30–34	−11.00	−78.17	30	34	319	2	Measured	14.03	22.62	0.15	0.03	0.246	This study
Peru Margin	PM-Stn460-6	−11.00	−78.59	6	6	1242	64	Measured	3.04	0.56	0.03	0.03	0.148	This study
Peru Margin	PM-Stn445-6–8	−11.00	−78.50	6	8	930	40	Measured	4.11	1.15	0.13	0.03	0.154	This study
Peru Margin	PM-Stn462-7	−11.00	−78.75	7	7	2025	93	Measured	2.71	0.86	0.10	0.03	0.137	This study
Peru Margin	PM-Stn459-14–18	−11.00	−78.43	14	18	697	13	Measured	5.53	59.39	0.35	0.03	0.162	This study
Peru Margin	PM-Stn460-8	−11.00	−78.59	8	8	1242	64	Measured	3.04	0.58	0.10	0.03	0.148	This study
Peru Margin	PM-Stn549-8	−11.00	−78.52	8	8	1005	42	Measured	3.33	0.70	0.11	0.03	0.152	This study
Peru Margin	PM-Stn445-8	−11.00	−78.50	8	8	930	40	Measured	4.11	0.97	0.15	0.03	0.154	This study
Peru Margin	PM-Stn445-10–12	−11.00	−78.50	10	12	930	40	Measured	4.27	1.06	0.12	0.03	0.154	This study
Peru Margin	PM-Stn449-12–14	−11.00	−78.17	12	14	319	2	Measured	13.45	27.11	0.20	0.03	0.246	This study
Peru Margin	PM-Stn470-12–14	−11.00	−77.94	12	14	145	2	Measured	6.46	52.95	0.33	0.03	0.294	This study
Peru Margin	PM-Stn455-14–18	−11.00	−78.32	14	18	465	2	Measured	6.82	21.41	0.07	0.03	0.175	This study
Peru Margin	PM-Stn481-14–18	−11.00	−78.24	14	18	376	2	Measured	3.47	13.61	0.12	0.03	0.194	This study

(*continued on next page*)

Table 1 (*continued*)

Location	Sample Name	Latitude (deg)	Longitude (deg)	Top depth in sediment (cm)	Bottom depth in sediment (cm)	Coring Water Dept (m)	Bottom Water O2 (μM)	O_2 estimate	OC (%)	Cd (μg/g)	δ^{114}Cd (‰)	2SD (‰)	$[Cd]_{surf}$ (nM)	Reference
Peru Margin	PM-Stn460-15	−11.00	−78.59	15	15	1242	64	Measured	2.62	0.64	0.11	0.03	0.148	This study
Peru Margin	PM-Stn549-15	−11.00	−78.52	14	14	1005	42	Measured	3.31	1.05	0.11	0.03	0.152	This study
Santa Barbara	SBB1-2CM	34.23	−120.03	1	2	594	1	Measured	3.08	1.10	0.09	0.03	0.071	This study
Santa Barbara	SBB2-3CM	34.23	−120.03	2	3	594	1	Measured	3.08	1.03	0.04	0.03	0.071	This study
Santa Barbara	SBB0.1CM	34.23	−120.03	0	0	594	1	Measured	3.08	1.27	0.11	0.03	0.071	This study
Santa Barbara	SBB3-4CM	34.23	−120.03	3	4	594	1	Measured	3.08	1.03	0.09	0.03	0.071	This study
W. Equ. Pacific	BJ8 103A	0.87	127.76	2	3	377	96	WOA18	3.08	0.10	−0.06	0.03	0.048	This study
W. Equ. Pacific	BJ8 MC98B	1.06	127.89	2	3	341	101	WOA18	2.35	0.10	0.00	0.03	0.044	This study
W. Equ. Pacific	BJ8-101B	0.87	127.76	2	3	377	96	WOA18	3.08	0.11	0.03	0.03	0.048	This study
W. Equ. Pacific	BJ8-105B	0.92	127.71	3	4	401	95	WOA18	3.61	0.13	0.03	0.03	0.048	This study
W. Equ. Pacific	BJ8-108A	0.94	127.69	0	1	272	102	WOA18	3.62	0.11	−0.01	0.03	0.048	This study
W. Equ. Pacific	BJ8-111A	0.99	127.74	0	1	268	102	WOA18	2.12	0.17	0.01	0.03	0.047	This study
W. Equ. Pacific	BJ8-MC106B	0.92	127.71	2	3	401	95	WOA18	3.30	0.11	0.03	0.03	0.048	This study
W. Equ. Pacific	BJ8-MC116A	0.97	127.81	0	2	472	95	WOA18	2.18	0.13	0.06	0.03	0.046	This study
W. Equ. Pacific	BJ8-MC94A	2.35	127.82	0	2	501	114	WOA18	0.37	0.17	−0.08	0.03	0.030	This study
W. Equ. Pacific	BJ8-MC96A	1.45	128.17	1	2	386	132	WOA18	0.76	0.09	−0.13	0.03	0.037	This study
Magadalena	MagD_0	23.50	−111.60	0	1	692	1	Measured	10.03	1.45	0.09	0.05	0.032	Chen (2021)
Pescadero	Pesc_2	24.30	−108.20	2	3	616	0	Measured	3.55	0.63	−0.02	0.05	0.053	Chen (2021)
San Nicolas Basin	MC37 2.5–3	32.80	−118.80	3	3	1750	15	Measured	4.92	0.53	−0.04	0.05	0.029	Chen (2021)
Santa Barbara	MC17_1	34.30	−120.00	1	2	493	2	Measured	3.01	0.85	−0.02	0.07	0.072	Chen (2021)
Santa Monica	8B3	33.70	−118.80	1	2	905	2	Measured	5.73	2.82	0.08	0.05	0.040	Chen (2021)
Soledad	Sol2_1	25.20	−112.70	1	2	544	0	Measured	6.47	1.84	0.06	0.08	0.034	Chen (2021)
Tanner	12B3	33.00	−119.70	1	2	1514	30	Measured	6.69	0.96	0.08	0.04	0.039	Chen (2021)

Additional data can be found in Table S2.

sulfide (H_2S) that is generated in the sediments can be released to the bottom water and accumulate to micromolar levels (Schunck et al., 2013; Scholz et al., 2016; Ohde, 2018). Furthermore, due to low sulfide solubility, CdS can precipitate in these waters with trace amounts of hydrogen sulfide (Davies-Colley et al., 1985; Rosenthal et al., 1995a). In essence, this creates an environment that can be, at times, both anoxic and sulfidic above the sediment. We measured twenty-six sediment samples from the margin shelf to the slope for water depths between 85 and 2025 m and were analyzed from a core depth between 0 and 35 cm. The sample sites span the reducing OMZ and the neighboring oxic water, with oxygen concentrations ranging from 0 μM to 93.4 μM. The sediments here were primarily made of fine-grained clay and have variable carbonate and calcareous ooze (Wu et al., 2020).

Sediment samples from the Santa Barbara Basin were collected as a part of the CALMEX Cruise in 2001 (R/V *New Horizon*). The Santa Barbara Basin is within the California Borderlands and has a sill depth of ≈475 m and a maximum depth of 627 m (Bernhard and Reimers, 1991). There is a limited exchange with water outside the basin; thus, the bottom water oxygen concentration is low, generally < 5 μM (Zheng et al., 2000). The core sites in this region have ferruginous porewaters, which indicates that iron and sulfate reduction are the dominant electron transfer pathways (McManus et al., 1997), similar to the Peru Margin. The region also has relatively high sedimentation rates (≈90 $mg/cm^2/yr$), which is partially attributed to high lithogenic input from the continent. The sediment samples were collected in the basin center, where the bottom water concentration was < 20 μM (Bernhard et al., 1997; Thunell et al., 1995). All the samples were collected near the core top but were from the same hole (between 0 and 3 cm). Thus, for some calculations, only the topmost sample was included. Sediments were primarily fine gained clay with some carbonate and calcareous ooze (Wu et al., 2020).

Samples from the Arabian Sea were collected on the R/V *Thomas Thompson* Cruises 41 and 47 in November 1994 and May 1995, with multicore samples taken between 16 and 19°N and 58 and 61°E. The Arabian Sea is a highly productive region with a dynamic oxygen minimum zone (OMZ) driven by monsoon cycling, water mass mixing, and several sources of micro and macronutrients. Because we do not have paired overlying water column data or porewater data, we used the closest cast in the World Ocean Database to determine the approximate O_2 concentration near where the sediment was collected at a similar bottom water depth. All of the samples were taken from near the core top (0–5 cm).

Western Equatorial Pacific samples were collected in July 2003 aboard the R/V *Baruna Jaya VIII*, Cruise 8 with a multicore and were subsequently stored in the WHOI Core Repository. The samples were taken in Kau Bay between the northern and northeastern edge of the Island of Halmahera at approximately 1N and 127E. The bay is highly productive and has bottom water oxygen concentrations of ≈100 μM, according to the nearest WOA18 hydrocast data (Boyer et al., 2022) and estimated at ≈80 μM O_2 based on field measurements from the 1980′s (van Aken and Verbeek, 1988; van der Weijden et al., 1989). Core top samples were taken at water depths between 250 and 500 m. All of the sediment samples were taken from 5 cm or shallower in the core and reflect coretop sediment. Sediment lithology was defined by calcareous ooze.

Finally, samples from the Angola and Namibian margin were collected aboard the R/V *Chain* in May 1970 and January 1974. The samples are stored in the WHOI Seafloor Samples Laboratory, and core top or near core top material was collected for analysis. The western coast of the South African margin is characterized by the upwelling of nutrient-rich waters with high productivity (Shannon and Nelson, 1996). Although biological activity leads to an intense oxygen minimum zone over large areas of the margin (Chapman and Shannon, 1987), the samples collected in these waters were collected at a water depth of ≈4000 m and were bathed by well-oxygenated waters. Like the samples from the Arabian Sea and Western Equatorial Pacific, we use the World Ocean Database 2018 to pair bottom water oxygen concentrations to these sediments. Sediment samples were taken between 0 and 5 cm below seafloor. The dominant lithology of the sediments is calcareous ooze.

2.2. Marine particulate matter

We examined Cd isotope compositions of marine particulate matter collected from the Ross Sea in the Southern Ocean (Fig. 1; Table 2). These samples were collected in January to February of 2011 aboard the R/V *Nathaniel B. Palmer* (NBP1101) using a large-volume *in situ* filtration system (McLane Research Laboratories, Inc.). Filters were acid cleaned prior to use following GEOTRACES protocols (Cutter et al., 2010). Between 97 and 439 L of seawater was pumped across each filter during pump deployment (mean of 298 L). Particulate samples were collected in two size fractions: a small size fraction (SSF; 0.8–51 μm), obtained using a 142 mm diameter polyethersulfone membrane filters, and a large size fraction (LSF; >51 μm), collected with a 142 mm diameter nylon screen. After collection, filters were sliced at sea using a ceramic blade in a laminar flow bench and placed in storage bags. Typically, 12.5 % (i.e., $^1/_8$) of the small size fraction filter was set aside for Cd isotope analysis, whereas 74 % of the nylon screen was sampled (ranging from 50 to 88 %). The samples in this study come from four stations with water depths ranging from 398 to 1,887 m, whereas the samples were collected between 0 and 600 m. No sediment samples accompanied these water column samples.

3. Materials and methods

3.1. Sample leaching

The total Cd content of sediment, $[Cd]_{total}$, can be considered as follows:

$$[Cd]_{total} = [Cd]_{lithogenic} + [Cd]_{biogenic} + [Cd]_{XS} \quad (1)$$

where $[Cd]_{lithogenic}$ is the lithogenic (or detrital) Cd in the sediment, $[Cd]_{biogenic}$ is the Cd that is bound with organic matter that is neither remineralized nor reprecipitated, and $[Cd]_{XS}$ is the concentration that is not supported by lithogenic or biogenic Cd. Here, a 17 h leach of 2 M HNO_3 at 60 ℃ was used to isolate: (i) Cd associated with organic matter ($Cd_{biogenic}$), (ii) Cd that was once hosted in organic matter, but was liberated to porewaters and recaptured as CdS, and (iii) CdS that formed pelagically in the water column of anoxic bottom waters in the presence of free H_2S. Both (ii) and (iii) constitute Cd_{XS}. Use of a leach ensured that biogenic and authigenic were sampled without liberating significant quantities of lithogenic Cd. Several treatments were tested before selecting the optimal leach (Section 4.1), which has been used in numerous other studies to avoid sampling detrital phases (e.g., Nielsen et al., 2011; Ostrander et al., 2017). We refer to the leachate fraction as $Cd_{leachable}$, whereby:

$$[Cd]_{leachable} \approx [Cd]_{total} - [Cd]_{lithogenic} \quad (2)$$

$$[Cd]_{leachable} \approx [Cd]_{biogenic} + [Cd]_{XS} \quad (3)$$

To differentiate between the biogenic and excess Cd, we calculated how much of the Cd was expected to be derived from organic material using a ratio of Cd to organic carbon:

$$[Cd]_{biogenic} = [OC] \times Cd:C \quad (4)$$

where [OC] is the total organic carbon measured in the sediment, and Cd:C is either estimated by an extended Redfield ratio (Ho et al., 2003) or measured ratios in field samples (Bourne et al., 2018). Thus,

$$[Cd]_{XS} \approx [Cd]_{leachable} - [OC] \times Cd:C \quad (5)$$

We assumed that the excess Cd, $[Cd]_{XS}$, was formed via one of two pathways. First, CdS can form near the sediment–seawater interface if the dissolved Cd encounters H_2S emanating from sediments. We refer to this as *pelagic CdS*. Alternatively, CdS can form within the sediment after the organic matter it was originally bound in is remineralized. If the liberated Cd encounters even trace amounts of H_2S in the porewater, it can be quantitatively reprecipitated. We refer to this as *porewater CdS*. Since the latter process is generally quantitative, it likely captures the Cd isotope composition of ambient porewater, and thus, organic matter δ^{114}Cd with no net Cd isotope fractionation. Both pelagic and porewater CdS formation would elevate Cd above what is supported by $[Cd]_{biogenic}$.

3.1.1. Sediment samples

All samples were prepared in the NIRVANA clean laboratory facilities at WHOI. Acids were double distilled in-house and were tested for their Cd content before use using methods described below. All water used in preparation was obtained from an 18.2 MΩ ultrapure, deionized water system (Milli-Q).

For each sample, approximately 20–30 mg of powdered sample was weighed into 7 mL perfluoroalkoxy vials (PFA, Savillex). The powder was treated with 2 M HNO_3 for 17 h at 60℃ and centrifuged to separate the detrital material (Nielsen et al., 2011; Owens et al., 2017). The refractory organic matter was oxidized by reacting concentrated HNO_3 at 250℃ for two hours in a pressurized microwave digestion system (Multiwave PRO; Anton Parr). After oxidation, an aliquot of each sample was analyzed on an iCAP Q ICP-MS (Thermo Fisher Scientific™) in the WHOI Plasma Facility to determine approximate Cd concentrations for initial spiking. A ^{111}Cd–^{113}Cd double spike was then added to each sample so that the spike-to-sample ratio (S:N) would be between 1 and 2. Spiked samples were then reconstituted in 1 M HCl for chromatography.

A two-stage anion-exchange chromatography was performed to separate Cd from the sample matrix. The separation technique was modified from Conway et al. (2013). In brief, the samples were loaded in 1 M HCl onto columns with pre-cleaned 500 μL AG MP-1 M anion-exchange resin (Bio-Rad™). Matrix elements were eluted in increasing molarities of HCl, and Cd was eluted using 2 M HNO_3. Next, the samples were dried down and reconstituted in Cl^- form and subsequently loaded in 1 M HCl onto pre-cleaned 180 μL AG MP-1 M anion exchange resin and the procedure repeated. Following column chemistry, residual organic material was removed with a liquid–liquid organic extraction (Murphy et al., 2016). Here, any excess organic material, either from the resin or carried over from organic-rich sediment samples, was extracted by adding 1.2 mL of optima-grade heptane to the eluted samples, shaking for 30 s, and allowing them to sit for three minutes. After sitting, the heptane was extracted and discarded, and the process was repeated. The samples were dried, reconstituted in 1.1 mL of 2 % HNO_3, and a subsample of 100 μL was taken to ascertain the spike-to-sample ratio (S:N), Cd concentration, and chemistry yields of the purified sample. Samples were diluted to achieve similar Cd concentrations (≈20 ng/mL sample-derived Cd) and organized such that samples with similar S: N were analyzed together. Cadmium isotope compositions were then measured and reported relative to spiked aliquots of NIST SRM 3108 possessing similar S: N to those of the samples. Given that samples were spiked prior to purification, Cd concentrations were determined simultaneously to isotope compositions.

To monitor the measurement precision and accuracy, aliquots of USGS SGR-1, NOD-A-1 and NOD-P-1 were processed alongside samples of unknown isotope composition. The USGS SGR-1 reference material was leached using the 2 M HNO_3 leach described above, whereas the USGS NOD-A-1 and NOD-P-1 underwent a 6 M HCl leach at 50℃ for 10 min before separation (Horner et al., 2010). After leaching, all standards were processed alongside the samples as per the protocols described above.

3.1.2. Marine particulate matter preparation

Particulate samples were leached in acid-cleaned PFA vials for 16 h in 0.6 M HCl at 80℃ (Bishop and Wood, 2008; Horner et al., 2017). The small size fraction filters were leached in 10 mL, whereas the nylon screens were leached in 50 mL. Samples were leached in 0.6 M HCl as this method does not appreciably dissolve the filter, but nonetheless results in near-quantitative recovery of many elements including P, Mn, Ba, Cd, and Sr (Bishop et al., 2012; Planquette and Sherrell, 2012). A 100 μL aliquot was taken from the leachate and Cd and P contents were determined by means of an external calibration using an ELEMENT 2 ICP-MS (ThermoFisher Scientific), also situated in the WHOI Plasma Facility. Samples were then evaporated to dryness, spiked with the same ^{111}Cd–^{113}Cd double spike to ensure a S:N of 1–2, and reconstituted in 1 mL of 1 M HCl for ion-exchange chromatography. The protocol was similar to that used for sediment samples; however, instead of a second pass through anion-exchange resin, the samples were instead reconstituted in 8 M HCl and passed through 180 μL of Eichrom TRU resin to remove any residual tin (Wombacher et al., 2003; Ripperger et al., 2007). Following this step, the samples were reconstituted in 2 % HNO_3 acid in preparation for mass spectrometry.

Table 2
Data for marine particulate matter from the Ross Sea.

Station	Depth	Lat	Lon	Bottom depth	$\delta^{114/110}$Cd (‰)	± 2 SE	[Cd]	[P]	$\delta^{114/110}$Cd (‰)	± 2 SE	[Cd]	[P]
	m	deg	deg	(m)	SSF	SSF	pM (SSF)	pM (SSF)	LSF	LSF	pM (LSF)	pM (LSF)
0	250	−76.50	170.00	737	−0.24	0.06	10	7169	0.18	0.04	2	1919
0	125	−76.50	170.00	737	−0.13	0.05	26	17,142	0.15	0.03	15	8349
0	50	−76.50	170.00	737	0.20	0.05	218	204,876	0.35	0.03	198	182,999
2	402	−75.19	174.00	428	0.16	0.19	6	4531	−0.19	0.03	2	2478
2	302	−75.19	174.00	428	−0.40	0.06	9	4846	−0.19	0.03	1	2032
2	212	−75.19	174.00	428	−0.49	0.05	11	5801	−0.14	0.03	2	2846
2	152	−75.19	174.00	428	−0.49	0.04	17	8015	−0.15	0.03	3	5701
2	82	−75.19	174.00	428	−0.27	0.06	15	17,653	−0.11	0.03	19	26,707
2	32	−75.19	174.00	428	−0.27	0.07	17	23,481	0.01	0.03	47	65,339
24	370	−74.14	176.66	398	−0.36	0.07	11	6157	−0.02	0.03	2	1968
24	210	−74.14	176.66	398	−0.49	0.04	8	4938	0.00	0.03	1	1299
24	120	−74.14	176.66	398	−0.13	0.05	12	10,701	0.05	0.03	31	28,381
24	80	−74.14	176.66	398	−0.17	0.04	25	23,483	0.07	0.03	66	68,832
24	30	−74.14	176.66	398	−0.06	0.05	78	73,479	0.11	0.03	47	71,616
14	600	−72.58	178.50	1887	−0.39	0.09	1	825	0.24	0.06	0	152
14	404	−72.58	178.50	1887	−0.41	0.08	3	712	−0.05	0.05	0	181
14	253	−72.58	178.50	1887	−0.46	0.06	6	1343	−0.22	0.03	1	453
14	150	−72.58	178.50	1887	−0.51	0.04	5	2281	−0.23	0.03	1	810
14	100	−72.58	178.50	1887	−0.36	0.06	11	6161	−0.21	0.03	3	5858
14	50	−72.58	178.50	1887	−0.27	0.04	92	44,207	−0.15	0.03	5	10,475

3.2. Cadmium isotope analysis

Cadmium isotope ratios were measured on a multi-collector inductively coupled mass spectrometer (MC-ICP-MS; ThermoFinnigan Neptune), situated in the WHOI Plasma Facility. Samples were aspirated into a desolvation system (Aridus II, CETAC) at approximately 140 μL minute^{-1}, and the resultant aerosol was introduced into the ion source using a 1 L minute^{-1} Ar carrier gas. The ion currents from 110 to 117 AMU were measured in 30 four-second integrations and processed with a MATLAB script to calculate the sample isotope composition from the spike–sample mixture and correct for isobaric interferences and instrumental mass fractionation. In this approach, isotope data were solved relative to the spike; however, Cd isotope data was reported relative to bracketing (spiked) aliquots of NIST SRM 3108 that were measured during the same analytical session (Abouchami et al., 2013). Within-run accuracy was monitored by analyzing appropriately spiked aliquots of BAM-I012, which we found possessed a Cd isotope composition of −1.33 ± 0.02 ‰ (±2 SD, n = 25). These values are identical, within uncertainty, to the inter-laboratory consensus value of δ^{114}Cd = −1.31 ± 0.04 ‰ (Abouchami et al., 2013). Long-term accuracy and precision were monitored by processing standard reference materials alongside sample unknowns.

4. Results

4.1. Reference standards and leach reproducibility

We performed a leaching experiment to examine three variables: reagent (HCl or HNO_3), molarity (2 M or concentrated), and temperature (60 or 135℃). All samples in the experiment were leached for 17 h. To assess the optimal leach, we examined the Cd/Al ratio in the leachate and the total amount of Cd that was recovered and compared it to the amount in the bulk sample.

Fig. 2 shows that nitric acid produced the greatest Cd/Al enrichment and both nitric leaches returned ≈700 ng/g of Cd, which is reasonable for the leachate given the $[Cd]_{Total}$ of between 900 and 1,200 ng/g (Jochum et al., 2005). Given the average Cd concentration of the upper continental crust is ≈100 ng/g (Wedepohl, 1995), we infer that these nitric acid leaches effectively extract the entire non-lithogenic, leachable Cd; between 800 and 1,100 ng/g are expected to be leachable, which overlaps with our value within uncertainty. We chose the 2 M HNO_3 at 60℃ as our optimal leach because of the aforementioned tests and because this leach procedure has been used in previous studies (e.g, Nielsen et al., 2011; Owens et al., 2017). The average SGR-1 leached concentration measured over the entire study for the 2 M HNO_3 at 60℃ was 704 ± 105 ng/g (2SD, n = 8). The SGR-1 USGS reference material had a mean δ^{114}Cd = −0.02 ± 0.03 ‰ (±2SD; n = 7). Although there is no literature data for the Cd isotope composition of leached SGR-1, the narrow range of δ^{114}Cd values implies that the leach performed similarly each time in agreement with the quantitative extraction of leachable Cd from the samples.

We also monitored whether the data were accurate by measuring two nodule standards: NOD-A-1 and NOD-P-1. The average leachable [Cd] of NOD-A-1 and NOD-P-1 was 5.6 ± 0.9 μg/g (2SD, n = 6) and 15.7 ± 1.7 μg/g (2SD, n = 6), respectively. The accepted values for these two reference materials are slightly more concentrated than our measured values, falling between 6.8–8 μg/g (NOD-A-1) and 20.9–23.3 μg/g (NOD-P-1) (Jochum et al., 2005; Schmitt et al., 2009). This slight difference is to be expected as our nodule treatment was a leach, rather than a total digest, and any undissolved material, presumably lithogenic in origin, was discarded. Our reported [Cd] values align with those found in Horner et al. (2010), who also used a 6 M HCl leach.

Despite the slightly lower Cd recoveries compared to those reported in the literature, both nodule standards exhibit Cd isotope compositions that are similar to consensus values. NOD-A-1 and NOD-P-1 exhibited an δ^{114}Cd = +0.11 ± 0.03 ‰ (n = 6) and +0.13 ± 0.03 ‰ (n = 6), respectively, which overlap with the recommended δ^{114}Cd of +0.129 ± 0.035 ‰ (NOD-A-1) and + 0.141 ± 0.052 ‰ (NOD-P-1; Lu et al., 2021). Assuming that our lower Cd recoveries relate to the presence of lithogenic material that is not sampled by our leach, it is unsurprising that our Cd isotope data for leached nodules is similar to that obtained from total digests. Lithogenic Cd typically exhibits δ^{114}Cd ≈ +0.1 ‰, and thus this pool of Cd exhibits a similar isotope composition to the (comparatively larger) leachable pool.

4.2. Cadmium concentration and isotope variations in sediment leachates

The 69 sediments in this study display leachable Cd concentrations between 0.09 and 59 μg g^{-1} (Table 1, Fig. 3a-b). Sediments with the highest and lowest $[Cd]_{leachable}$ are from the Peru Upwelling Region and the Western Equatorial Pacific, respectively.

The Cd isotope composition of the samples fall between δ^{114}Cd = −0.18 and + 0.35 ‰ (Table 1). Except for the Peru Margin, the measured isotope compositions are similar within a given region. The heaviest isotope compositions occur in the Peru Margin at low bottom water oxygen concentrations and the lightest in the Namibian Margin at high oxygen concentrations.

4.3. Marine particulate Cd concentrations and isotopes from the Ross Sea

Four stations in the Ross Sea were selected to measure particulate δ^{114}Cd ($p\delta^{114}$Cd). The profiles of small size fraction (SSF) $p\delta^{114}$Cd are like those observed in the Northeast Pacific by Janssen et al. (2019), whereby the surface $p\delta^{114}$Cd sample is the heaviest for all four stations, and the $p\delta^{114}$Cd becomes lighter with depth (Fig. 4e-h). For three of the stations, the deepest SSF sample tends to return towards heavier values, although the deepest sample exhibits lighter δ^{114}Cd than the surface value. The only profile that does not show this trend is Station 0, but this station was not sampled deeper than 250 m, so we cannot rule out the possibility that it would have followed the same trends seen at the other stations. The O_2 profiles for Station 2, 14 and 24 are shown in Fig. 4(b-d). Unlike the samples from the Northeast Pacific, all of the water column profiles in the Ross Sea are well oxygenated, with $[O_2]$ > 175 μM. Particulate Cd concentrations (p[Cd]) for all 8 profiles show highest concentrations in the surface and decrease with depth (Fig. 4i-l), similar to profiles of particulate P (Fig. 4m-b; Bishop and Wood, 2008).

The large size fraction particles (LSF) follow the same trends that were observed in the SSF (Fig. 4). Stations 0, 2 and 24 show that the samples become isotopically lighter with depth, but not to the same extent as the SSF particles and are often within the uncertainty of the other samples collected at the same station. Station 14, the most offshore sampling location, shows the largest change of Cd isotopes with depth: the top 250 m of water have a similar $p\delta^{114}$Cd value, whereas deeper samples become isotopically heavier. Indeed, the deepest sample at St.14, from 600 m, is offset by + 0.40 ‰ relative to the shallowest LSF sample.

5. Discussion

5.1. Cadmium sulfide incorporation into marine sediments

5.1.1. Evidence for cadmium sulfide incorporation into sediments

As described previously, CdS can be incorporated into sediments via two mechanisms: *pelagic precipitation* from seawater and *porewater precipitation* within the sediment. In the first mechanism, Cd can precipitate directly out of seawater under anoxic conditions with a permanent or transient source of dissolved H_2S. In the second, Cd that was originally bound by organic matter can be transferred into CdS if organic matter is remineralized and the liberated Cd is reprecipitated from sulfide-containing porewaters (Gobeil et al., 1987; McCorkle and Klinkhammer, 1991). Porewater precipitation can elevate the amount of Cd in the sediment relative to that expected from OC in the sediment and is

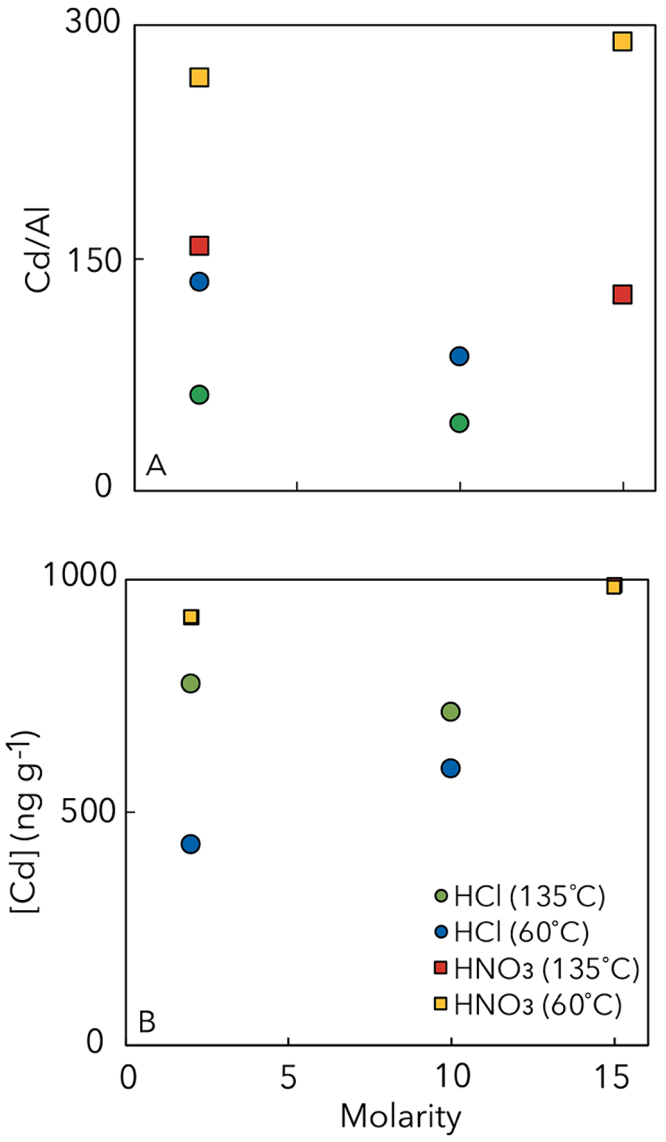

Fig. 2. Results from the leach experiment. Aliquots of SGR-1 were leached under three conditions: nitric acid or hydrochloric acid, 60℃ or 135℃, and 2, 10 or 15 M. The optimal leach (2 M nitric acid at 60℃) was selected based on an enhanced Cd/Al ratio, [Cd] in the leachate, and previous use as a leach in similar studies. Data used to make this table is available in Table S1.

likely to occur in most sedimentary environments. We analyzed samples from three regions with anoxic bottom waters: the Peru Margin, the Cariaco Basin, and the Black Sea, each with an increasing degree of oceanographic restriction. The Black Sea and Cariaco Basin are both euxinic (i.e., anoxic and sulfidic). Meanwhile, although the Peru Margin is not classified as a euxinic basin, H_2S may episodically accumulate in the bottom waters when the conditions become stagnant, and nitrate and nitrite are depleted.

A recent study by Plass et al., 2020 used benthic chamber incubation data to show that Cd sulfides could precipitate in near-bottom waters and could account for up to 60 % of the excess Cd accumulation in Peru Margin sediments. Subsequently, sequential extraction data provided evidence that Cd sulfide precipitation from the bottom waters was important to account for Cd delivery and burial in the sediment (Plass et al., 2021). While the extraction data illustrated that most of the Cd hosted in the sediment was present as CdS, the authors of the study were unable to differentiate whether the CdS was formed in the water column near the sediment–water interface or within the porewaters. The authors calculated the amount of Cd in the sediment from both the organic carbon rain rate and the carbon accumulation rate at 10 cm in the sediment from the same stations along the Peruvian transect using data from other studies (Dale et al., 2015, 2021). We take a similar approach for a direct comparison. We multiply our leachable Cd concentrations by the published MAR (Dale et al., 2021) from the same station in the Peruvian transect, noting that only five of our samples had an associated MAR. Next, we estimate the Cd arriving in the rain rate and the accumulation rate at 10 cm by using an average Cd:C phytoplankton ratio (Ho et al., 2003; Moore et al., 2013). The amount of Cd in the sediment that arrived from organic matter should fall between the rain rate and the accumulation rate. We find that for sediments that fall within or near the OMZ (85 m to 697 m), Cd from the rain rate of OC can account for a maximum of ≈20 % of the Cd hosted in the leachable fraction (Table 3, Fig. 5). The Cd fluxes that we estimate in the sediment are far higher than can be explained by organic matter rain rates alone. Thus, our data confirms earlier findings by Plass et al. (2020).

Fig. 6 shows that the Cd:OC relationship develops as the samples transition from sediment that is bathed in anoxic bottom water where CdS may form to sediment that is beneath oxic waters where CdS is unlikely to be delivered pelagically to the sediment. Two sediment samples show enrichment of Cd outside of the defined OMZ (i.e., between 100 and 500 m water depth). However, both of these samples fall just outside of the OMZ (at 85 m and 697 m). Because these samples are close to the OMZ boundary, we suggest that they formed from the same processes that are driving CdS formation within the core of the OMZ.

Unlike in the Peru Margin, the samples from the Black Sea and the Cariaco Basin do not suggest that pelagic precipitation of CdS is an important delivery mechanism. The Cariaco Basin samples have Cd:OC values of about 4 μmol Cd/ mol OC, which is within the range of Cd:OC values that are supported by organic matter delivery (Ho et al., 2003; Bourne et al., 2018). Likewise, the Cd:OC ratio in the Black Sea can be reasonably explained by organic delivery of Cd as well (i.e., ≈2 μmol Cd/ mol OC; Fig. 3).

Since the Black Sea and Cariaco Basin have anoxic bottom waters with persistent free sulfide (Section 2.1), it may at first be surprising that they do not exhibit evidence for pelagic precipitation of CdS to the sediment. However, these data suggest that the degree of restriction likely influences whether CdS is the primary delivery vector of Cd to sediments within a basin. Unlike the Peru Margin, the Cariaco Basin and the Black Sea are restricted and have limited mixing with open ocean seawater. We suggest that any dissolved Cd that does enter into the euxinic bottom waters may be stripped out of the water column soon after it encounters free sulfide. This theory is supported by the low Cd concentrations observed below the chemocline in both the Black Sea and the Cariaco Basin. Studies have shown that in the modern Cariaco Basin, Cd concentrations of water below the chemocline are generally <0.02 nM Cd, and in the modern Black Sea concentrations are even lower (e.g., <0.01 nM; Tankéré et al., 2001; Little et al., 2015). The sediment samples measured in this study all come from substantially deeper than the chemocline. Therefore, as there is no upwelled supply of Cd, we expect the Cd that formed CdS to be stripped out and deposited in the sediment closer to where the Cd first encounters the euxinic water (i.e., in proximity to the edges of the basin). For example, Little et al. (2015) suggested that a minor amount of seawater-derived CdS was present in sediment from a core in the Cariaco Basin located near to the Tortuga bank between two local deepwater maxima (Fig. 1). However, in the other samples measured in the Cariaco Basin and the Black Sea, it appears that little, if any, CdS makes it to the sediments through pelagic precipitation because of the low Cd supply.

5.1.2. Impact of cadmium sulfide precipitation on cadmium isotope compositions

As suggested in Section 5.1.1, we expect the leachable Cd in sediments from the Cariaco Basin and the Black Sea to primarily reflect organically derived Cd, not pelagic sulfide precipitation. The Cariaco

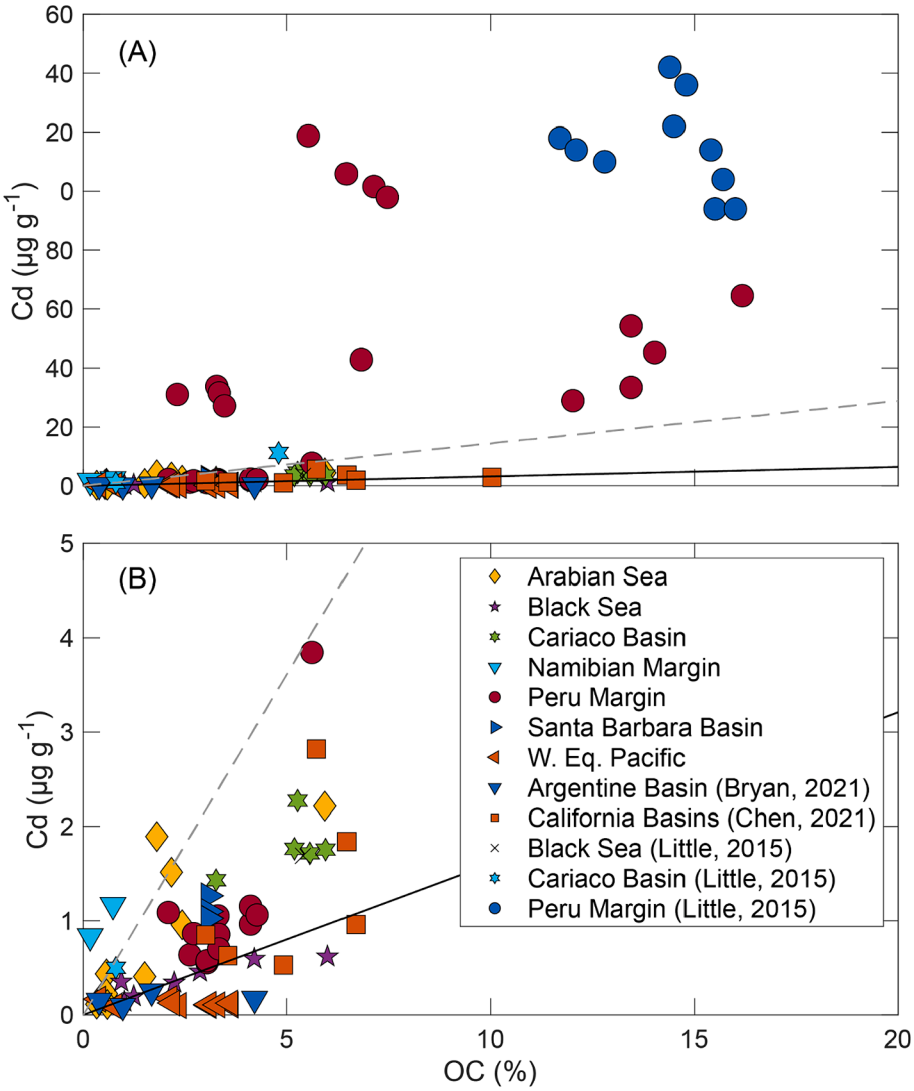

Fig. 3. Crossplots showing sedimentary Cd concentrations as a function of organic carbon content. (A) All leachable Cd concentrations versus organic carbon concentrations. For comparison, the dashed gray line is the average Cd:C ratio from euphotic particles in the Peru Margin (7.66×10^{-6}; Bourne et al., 2018) the solid black line is the Cd:C ratio in the 'average' phytoplankton (1.69×10^{-6}; Ho et al., 2003). Samples in the Peru Margin have increased Cd concentrations, suggesting an input of excess CdS (B) Zoomed in on the leachable Cd concentrations that fall between 0 and 5 µg g^{-1}.

Basin sediment Cd isotope compositions are, on average, $\delta^{114}Cd = +0.28 \pm 0.03$ ‰ (n = 12). The isotope composition of the Black Sea sediments is isotopically lighter than the Cariaco Basin sediments, with a mean composition of = +0.11 ± 0.05 ‰ (n = 5). We suggest that the restricted nature of both basins limits the physical mixing of Cd-replete waters into the surface as there is no shortage of sulfide in the water column. Therefore, the Cd isotope composition of organic matter produced in the surface waters most likely reflects the source of Cd to each region (i.e., open ocean seawater with $\delta^{114}Cd = +0.25$ ‰ for the Cariaco Basin and riverine inputs with $\delta^{114}Cd \approx +0.1$ ‰ in the Black Sea). Isotope fractionation during biological uptake is also possible, although less likely given the similarities with the Cd isotope compositions of likely Cd source material.

Unlike the Cariaco Basin and the Black Sea, the high excess Cd in the Peru Margin sediments is evidence for pelagic precipitation of cadmium sulfides. This also impacts the distribution of sedimentary $\delta^{114}Cd$ (Fig. 7). Samples within the OMZ, with anoxic bottom waters and which experience transient sulfidic water, exhibit $\delta^{114}Cd$ between +0.12 and +0.35 ‰. In the oxic bottom waters outside the OMZ, with no evidence of free sulfide, bottom water oxygen > 20 µM O_2, and deeper than 700 m, $\delta^{114}Cd$ spans a narrower range from +0.03 to +0.15 ‰, with an average value of +0.11 ‰.

We propose that the isotope composition of the sediments throughout the Peru Margin reflects the combined compositions of CdS precipitated directly from seawater and Cd that was incorporated into organic matter. While the OMZ portion is dominated by pelagic CdS precipitation, the oxic region outside of the OMZ is dominated by Cd incorporation into organic matter. The isotope composition of Cd in the oxic portion below the core of the OMZ, therefore, is set by biological utilization of Cd in the surface waters and any potential fractionation that occurs during remineralization as the organic matter transits to the seafloor.

In Section 5.1.1, we argued that the predominant formation of excess Cd in the sediment within the OMZ is from CdS that precipitates in the bottom waters. This finding is corroborated by the differences in isotope composition of these two regions. Cadmium sulfide reprecipitation in the porewater is expected to quantitatively capture Cd from organic matter. If porewater CdS formation were a dominant source in the Peru Margin, we would not expect large deviations in the isotope compositions of the sediments within the OMZ versus those in the oxic regions.

We can determine the relative importance of CdS formation and Cd that is still bound by organic matter by examining sedimentary Cd:OC

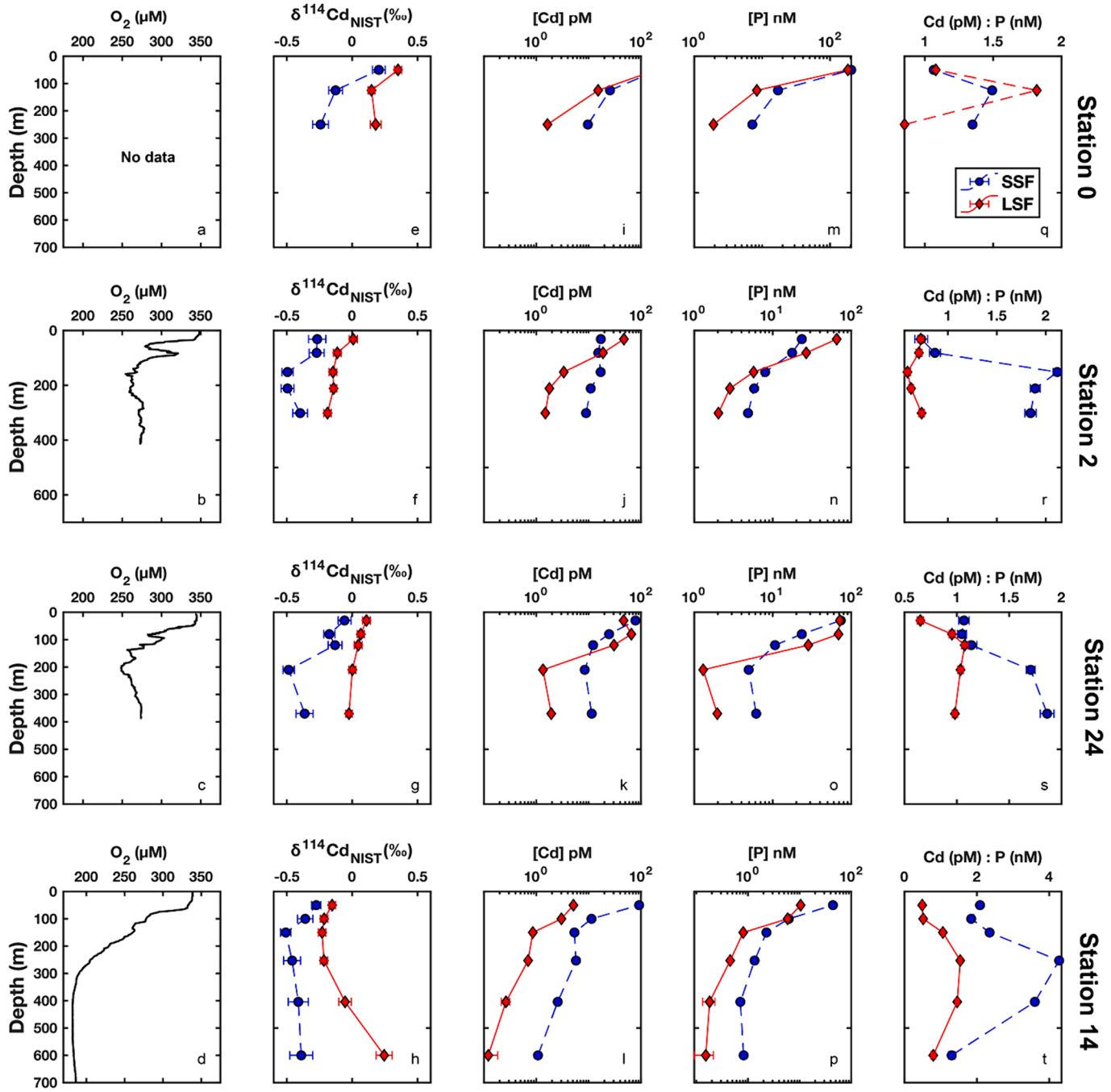

Fig. 4. Multi-element geochemical and Cd isotope data for particulate samples from the Ross Sea . The first column shows dissolved O_2 concentration of the water column at stations 0, 2, 24 and 14 (a-d). The second column shows particulate δ^{114}Cd (‰) (e-h). The third and fourth columns show the Cd concentration and P concentrations, respectively (i-p). The fifth column shows particulate Cd:P. The large size fraction particles are shown in red diamonds with a solid line, the small-size fraction particles are shown in a blue circle with a dashed line.

ratios. Values for Cd:OC ratios from organic-derived sources range between 1.69 and 7.66 μmol Cd: mol C. Here, we use a ratio of 7.66 because those were the ratios measured in Peruvian samples (Bourne et al., 2018). We construct a mixing relationship between the sulfide and organic matter components. We observe that our two samples dominated by excess cadmium (i.e., greater than 90 % excess Cd) possess a mean δ^{114}Cd value of + 0.31 ± 0.03 ‰ (Fig. 8). Our organic-matter dominated samples (i.e., 0 % excess Cd) have an average δ^{114}Cd of + 0.11 ± 0.03 ‰ (2SD; n = 8). Two recent studies measured that the dissolved seawater Cd isotope composition in the Peru Margin above 500 m of water depth is ≈+0.5 ‰ (John et al., 2018; Xie et al., 2019). This offset implies a Cd isotope fractionation, $\Delta^{114}Cd_{CdS\text{-}medium}$, of approximately –0.2 ‰. This finding aligns with previous laboratory studies that reported an isotope fractionation factor for CdS precipitation from an aqueous solution, $\Delta^{114}Cd_{CdS\text{-}medium}$, of approximately –0.3 ‰ (Guinoiseau et al., 2018).

Fig. 8 shows that some of the samples deviate from the trend between δ^{114}Cd and OC:Cd. We suggest that these samples may have more influence from reprecipitation of Cd that was derived from organic matter and this reprecipitation could be the reason for the lighter Cd isotope signatures.

Table 3
Cd excess and the range of contributions that can reasonably expected to be from Cd that arrived in association with organic carbon.

Station	Depth (cm)	Type	MAR	POC rain rate	POC accumulation rate at 10 cm	Rain Rate (min)	Accumulation Rate at 10 cm (max)	Rain Rate (min)	Accumulation Rate at 10 cm (max)	Excess
			g m^{-2} yr^{-1} [a]	mmol C m^{-2} d^{-1}[b]	g C m − 2 yr − 1b	μmol Cd m^{-2} yr^{-1}[c]	μmol Cd m^{-2} yr^{-1}[c]	μmol Cd m^{-2} yr^{-1}[d]	μmol Cd m^{-2} yr^{-1}[d]	μmol Cd m^{-2} yr^{-1}
M77-1 549 *MUC53	7	Oxic	390	5.9	16	3.6	2.3	11.6	7.2	3
M77-1 BIGO-05	10	OMZ	1400	15.3	31	9.4	4.4	30.2	13.9	193.4
M77-1 MUC19	8–10	OMZ	190	9.8	17	6	2.4	19.3	7.6	54.5
M77-1 MUC25	14–18	Transition	420	9	32	5.6	4.5	17.7	14.4	221.9
M77-1 MUC33	14–18	OMZ	270	14	44	8.6	6.2	27.6	19.8	32.7

[a] from (Dale et al., 2021).
[b] from (Dale et al., 2015).
[c] Value determined by multiplying the Cd:C ratio in average phytoplankton (Ho et al., 2003) with the particulate organic carbon rain rates (max[b]) value and the organic carbon accumulation rates (min[b]). The excess Cd is calculated by multiplying the MAR by the measured leached Cd. A similar calculation is found in (Plass et al., 2021).
[d] Value Same as above, but the Cd:C ratio in Peru Particles (Bourne et al., 2018) was used.

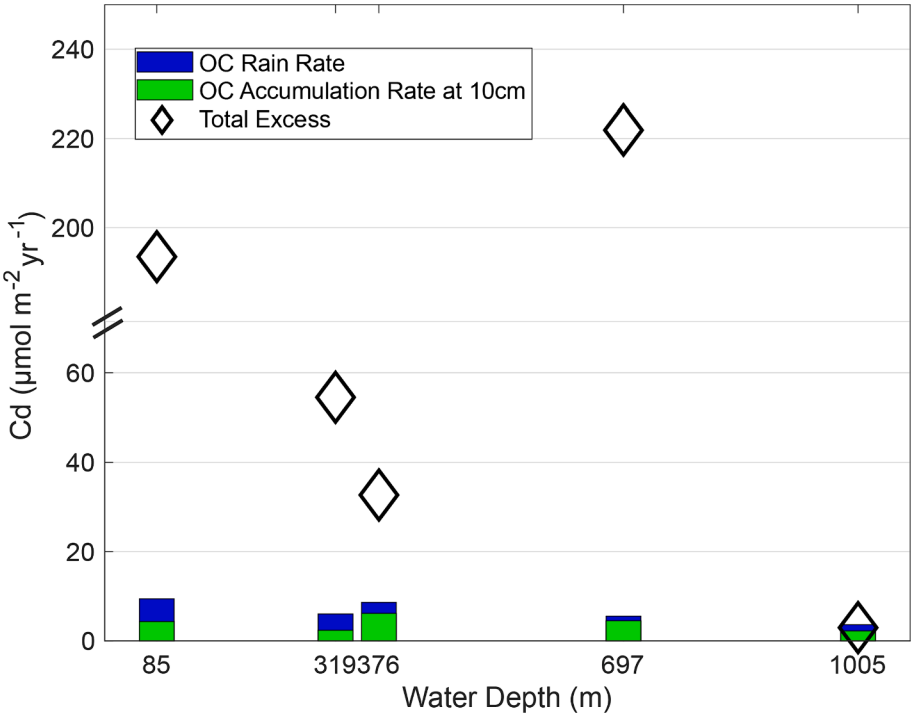

Fig. 5. Calculation of sedimentary Cd excess along the Peru Margin. Cadmium excess accumulation is shown by the diamonds. Cadmium contribution can come from Cd incorporation from organic matter, re-capture in porewater by sulfide, and CdS pelagic precipitation in the bottom water. The entire bar represents the total Cd that can come from the OC rain rate (assuming all Cd is captured either with OC or via porewater precipitation) while the green represents what is expected from OC that is accumulated in the sediment at 10 cm (allowing for Cd to be remineralized without recapture). The reader is referred to Plass et al. (2021) to see an analogous figure in the same region. In order of left to right, the Peru Margin stations collected along the 11S transect are Station 568, 449, 481, 459, 549. More information on these stations can be found in Dale et al. (2015) and Scholz et al. (2011). The station numbering scheme is from Scholz et al. (2011).

5.1.3. Is CdS formation important to the global marine mass balance of Cd?

The two euxinic (Black Sea and Cariaco Basin) and one anoxic and intermittently sulfidic (Peru Margin) regions highlight how the δ^{114}Cd of sediments depends on redox conditions, organic matter delivery, and regional hydrography. The presence of free sulfide and a supply of dissolved Cd to the bottom water results in elevated Cd concentrations and heavier Cd isotope values. However, free sulfide without a supply of dissolved Cd prevents significant CdS from forming. Regions where both these conditions are met—anoxic, with at least periodic H_2S accumulation in the bottom waters *and* a supply of Cd—are relatively rare compared to other margins where the bottom waters tend to have measurable oxygen concentrations and/or no evidence for free sulfide in the bottom waters. Indeed, the only place found to date with ample evidence for the formation of CdS from seawater is on the Peru Margin. It is likely that the Namibian margin, which also has sulfidic events (Brüchert et al., 2006; Currie et al., 2018), undergoes a similar CdS drawdown. While two samples from this region were measured, they were obtained from an oxic portion and not representative of an otherwise intermittently sulfidic region. Performing an analogous characterization of the Cd isotope composition of sediments deposited along the Namibian margin would help to discern whether the patterns observed in the Peruvian upwelling system are representative of other low-oxygen settings. Despite not having samples from the region of the Namibian margin that experience sulfidic events, we did measure several samples from the low oxygen portions of the Arabian Sea and the California margin. We do not see any similar excesses of Cd that require

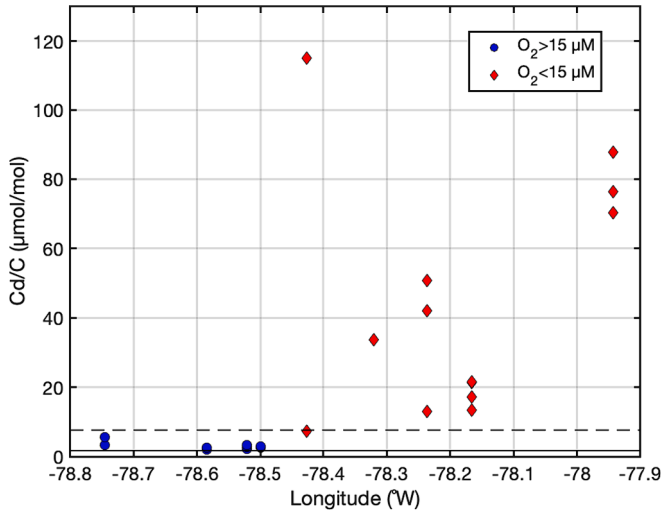

Fig. 6. Cd:OC composition in the sediment across the 11 °S Peru Margin transect. Data color coded by bottom water oxygen content (i.e., < 15 µM as red diamonds and > 15 µM as blue circles). The lines represent the range of expected Cd:OC via delivery with organic matter based on previous studies (i.e., solid line: Ho et al., 2003; dotted line: Bourne et al., 2018). The data was collected along the 11S transect in the Peru Upwelling Zone. Station numbering is found in Table 1 under sample name.

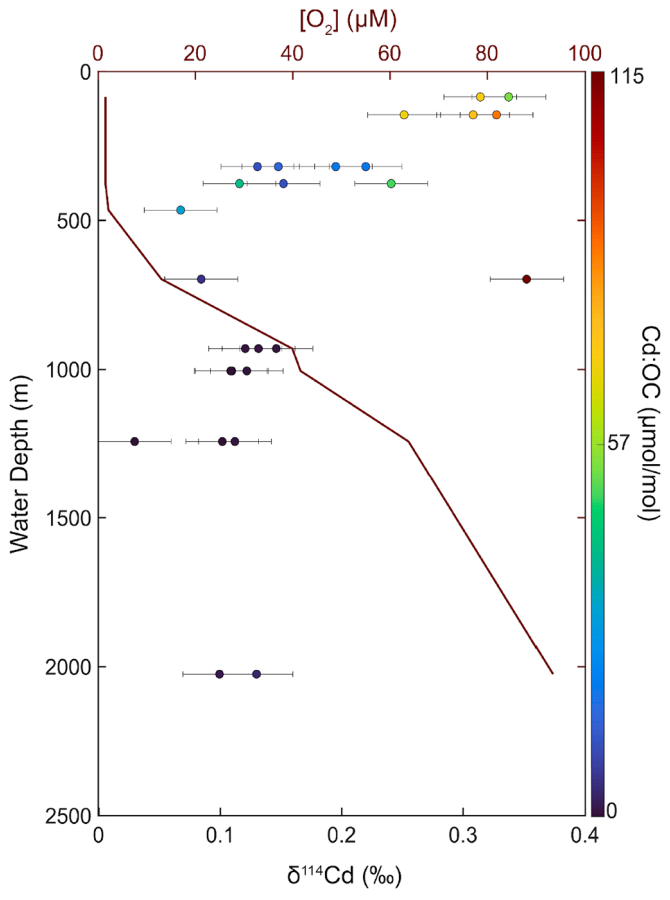

Fig. 7. Core-top Cd isotope compositions as a function of water depth for the Peru Margin samples (see Table 1 for sample details). The top axis and red line show the bottom water oxygen content against water depth. Data points show the isotope composition relative to water depth. The color bar shows the Cd:OC ratios. The darkest blue values are wholly supported by organic matter whereas all other colors have excess Cd.

precipitation of CdS from bottom waters. Therefore, our data indicate that pelagic CdS precipitation is not a general feature of OMZs and that a buildup of free sulfide in bottom waters is essential for pelagic CdS formation to significantly contribute to Cd sedimentation.

To estimate the amount of pelagic CdS that is buried in sediment on the Peru Margin we approximate the amount of CdS that may be expected to form during a sulfidic event. Schunck et al. (2013) reported a sulfidic plume in the Peru Margin that was 5,500 km^2 in size from 12S to 14S, and was the largest plume observed in ocean waters. Jahnke (2010) suggests that the OC flux to the Peru Margin area is about 0.59 mol OC m^{-2} yr^{-1}, which would correspond to a deposition of 4.5 µmol Cd m^{-2} yr^{-1}, using a Cd:OC molar ratio of 7.6 µmol mol^{-1}. On average, our samples in the Peru Margin that show evidence of CdS deposition are between 2 and 15 times higher than what is expected from organic matter alone, with an average value of 6 times higher. Thus, the Cd deposition in that region would be a maximum of 3.7×10^5 mol Cd yr^{-1}. However, if the total global organic matter flux of Cd is about 6.2×10^7 mol Cd yr^{-1} (Chen et al., 2021) this would only account for 0.6 % of global Cd deposition. If the same process exists to the same extent in the Namibian margin, this would still account for ≈1.2 % of global Cd deposition. Thus, we conclude that pelagic CdS deposition is, overall, insignificant in the global marine Cd cycle. For this reason, we turn to regions with oxygen at the sediment–water interface to understand the global Cd fluxes into the sediment.

5.2. Cadmium deposition under oxic conditions

5.2.1. Cadmium concentrations and $\delta^{114}Cd$ in oxic environments

The quantity of Cd deposited in sediments underlying oxic regions depends primarily on the amount of organic matter reaching the seafloor (Fig. 3b). While there is no evidence for pelagic precipitation of CdS out of bottom water in these regions, it is possible that some CdS may form in porewaters after remineralization of organic matter within the sediments (i.e., porewater Cd). The two lines included in Fig. 3 are the Cd:OC ratio expected from the extended Redfield value (Ho et al., 2003) and measured field particle data (Bourne et al., 2018). All our data fit on or near these estimated values, so a significant Cd subsidy from pelagic or porewater CdS is not needed to explain the data. Although we cannot conclusively state that these samples are free from CdS formation during remineralization of organic matter, such effects must be minor as there is limited excess Cd in these samples. Overall, we consider it unlikely that porewater CdS precipitation would significantly impact the measured leachable sediment Cd isotope compositions, as sulfide in the porewater is expected to quantitatively capture any liberated Cd. Although we acknowledge that, under certain conditions, porewater CdS may not be quantitative, or Cd may precipitate in an oxide phase under oxic porewater conditions, studies such as Rosenthal (1995a) propose that CdS formation can occur even in suboxic sediments where H_2S is not yet detected. Rosenthal (1995a) suggests that free sulfide can diffuse upward, supporting sulfide precipitation. Additionally, anoxic microhabitats within the sediment may provide a local source of sulfide. Therefore, we infer that the majority of Cd released from the degradation of organic matter in sediments is eventually re-captured as CdS. However, it is important for future research to investigate oxic porewaters to determine whether the formation of Cd oxides is globally significant and whether non-quantitative CdS formation is widespread, potentially imparting a fractionation similar to what has been suggested for ZnS precipitation in sediments (Zhang et al., 2021).

The range of $\delta^{114}Cd$ in the 34 oxic sediment samples falls between −0.18 and +0.25 ‰. To estimate the global average Cd isotope composition of sediment organic matter, it is important to understand what processes may control the isotope variation of the organic matter that arrives at the seafloor. Because $\delta^{114}Cd$ in seawater and marine particles are thought to be controlled by factors such as primary productivity, relative nutrient utilization in surface waters, and the length scale and intensity of remineralization, we performed a multiple linear

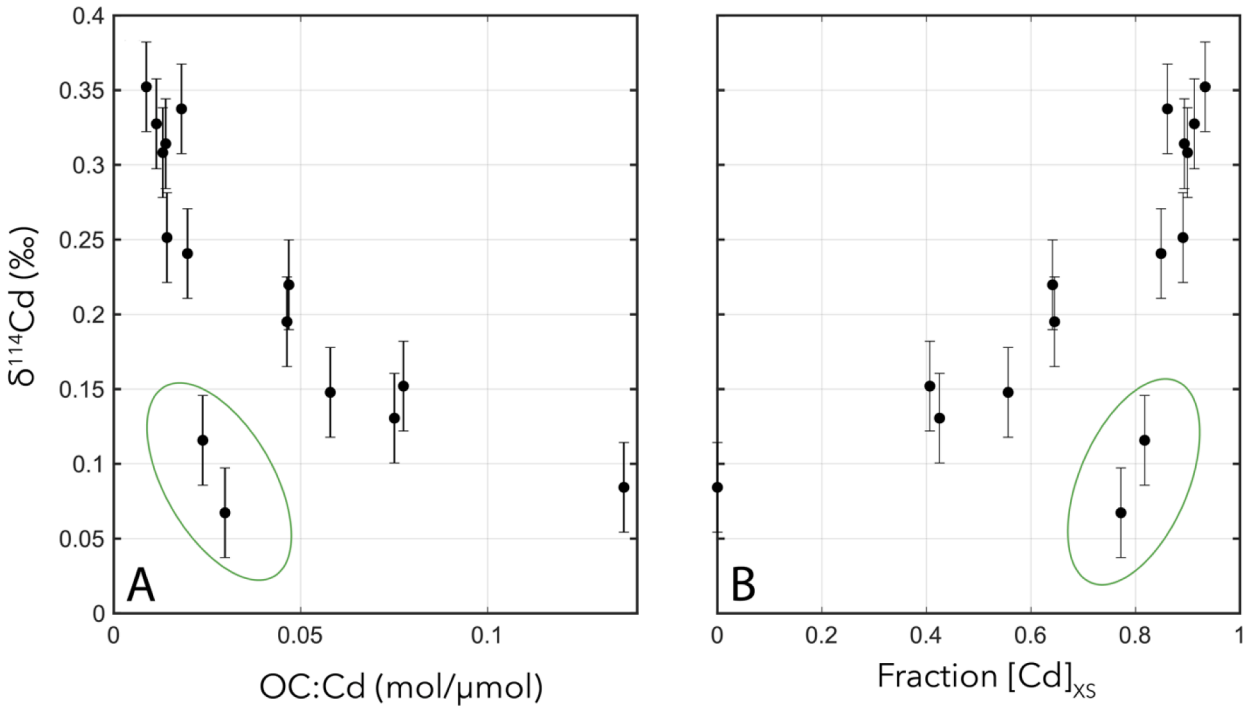

Fig. 8. Core top isotope evidence for Cd supply in excess of organic material. (A) Shows the relationship between δ^{114}Cd and Cd:OC ratio for all samples that have Cd concentrations that are higher than those supported by organic matter input alone (i.e., have evidence for pelagicporewater CdS input). (B) Assumes that any Cd:OC that is in excess of the Cd predicted from molar Cd:C ratio in Bourne et al. (2018) is from input of CdS. The fraction of this excess Cd is shown versus δ^{114}Cd. Two points fall below the isotope value predicted by pelagic precipitation (circled). We posit that these samples may have CdS that forms from organic matter remineralization (porewater CdS precipitation) instead of bottom water CdS precipitation.

regression analysis using variables related to these properties: solid-phase Cd concentrations from the leach ($[Cd]_{leachable}$), the dissolved Cd concentration in surface waters above a sediment sample ($[Cd]_{surface}$), the dissolved O_2 concentration in bottom water at the site of sedimentation ($[O_2]_{bw}$), the solid-phase OC content of the sediment (OC %), and the water depth overlying the sediment core (z). We used this analysis to determine which of these variables are most strongly related to the leachable Cd isotope composition of the sediment. The analysis involved compiling the oxic data into the following Eq. (6):

$$\delta^{114}Cd_{sed} = \boldsymbol{\alpha} \times [Cd]_{leachable} + \beta \times [Cd]_{surface} + \boldsymbol{\gamma} \times [O_2]_{bw} + \varepsilon \times waterdepth + \zeta \times OC(\%) + b \quad (6)$$

where are $\boldsymbol{\alpha}$, β, $\boldsymbol{\gamma}$, ε, and ζ are the coefficients subject to optimization and b is a constant. All parameters were measured or, in the case of $[O_2]_{bw}$, extrapolated from the WOA 2018. All values used in the analysis are compiled in Supplementary Tables S2 and S3.

We optimized the equations for every combination of parameters (n = 63 equations) to explore the range of the parameter space. We determined which coefficients provided the best offset by minimizing the root mean squared deviation between the measured and predicted sedimentary Cd isotope values. The results reveal that only two parameters, $[Cd]_{surface}$ and $[O_2]_{bw}$, are significantly related to the Cd isotope composition of the sediment (Table S3). We performed an F-test to identify that using the model that includes both $[Cd]_{surface}$ and $[O_2]_{bw}$ are not statistically different from using the model with all of the variables. However, using the two parameters together is statistically distinct from using the two parameters separately. While these variables appear to be codependent (i.e., they have a better correlation with the δ^{114}Cd of the sediment when used together than when applied independently) we will treat them as both independent parameters and codependent variables. We recognize that these variables likely do depend on one another, but to understand their role theoretically, it is necessary to explore them independently to better understand what physical underpinning may drive their relationship to δ^{114}Cd. We thus examined three models that predict the isotope composition of the sediment: linear regressions using each of the variables individually and a linear combination of the two variables.

The first two models can be described with a simple linear regression: The r^2 value of $[Cd]_{surface}$ and δ^{114}Cd is 0.4 and the r^2 value of $[O_2]_{bw}$ and δ^{114}Cd is 0.6. We can quantify the significance of r^2 by determining the likelihood that correlations are statistically significant. We use statistical tables given in Taylor (1982) to determine the correlation of individual parameters with the isotope composition. We find that the surface water Cd concentrations and sediment isotope compositions have a 92 % probability of being meaningfully correlated. Sedimentary Cd isotope data and bottom-water $[O_2]$ have a 99.5 % chance of being meaningfully correlated. We also calculate an adjusted r^2 of 0.65 for the combination of both variables and find greater than 99.5 % probability that both variables are significantly correlated with δ^{114}Cd of the sediments.

Though these parameters are correlated with our sedimentary data, the mechanisms underpinning these correlations are complex. In the following section, we examine the extent to which these correlations may be used to predict the isotope composition of the sediment.

5.2.2. *Relationship between surface seawater [Cd] and sedimentary δ^{114}Cd*

The linear regression shows that surface Cd concentrations are correlated with δ^{114}Cd (Fig. 9). The correlation suggests that as the Cd surface concentrations increase, sedimentary δ^{114}Cd increases. However, this behavior is the opposite to the relationship expected based on biological uptake of Cd from surface seawater and export of this signature to the sediments with no further modifications. Our sediment samples underlie surface waters with some of the lowest Cd concentrations observed in global seawater (i.e., <0.15 nM). Extrapolating our observed relationship over the entire range of surface Cd concentrations in the ocean (up to 1.2 nM), suggests that sedimentary organic matter at the highest surface water [Cd] could reach values of ≈+1.3 ‰. Such

values are unrealistic, underscoring a bias in our sample set toward samples underlying low surface Cd concentrations. Instead, we suggest that the Cd isotope compositions of sediments underlying Cd-depleted surface seawater behave differently to those underlying Cd-replete regions. This is analogous to the observations made in the water column. Indeed, cadmium isotope fractionation in seawater varies between high-[Cd] HNLC regions, such as the Subarctic North Pacific and Southern Oceans (e.g., Sieber et al., 2023; Xue et al., 2013), and low-[Cd] oligotrophic regions, including the South Pacific and South Atlantic (Gault-Ringold et al., 2012; Xie et al., 2017; George et al., 2019).

Many explanations have been proposed for these different fractionation behaviors. In regions with low concentrations of Cd in the surface water, the surface isotope composition may be increasingly influenced by vertical inputs of Cd from one of two possible inputs. First, additions of Cd from aerosols may influence the Cd isotope composition of surface waters. Aeolian deposition of Cd is isotopically light, ranging from −1.91 ‰ −0.07 ‰ (e.g., Sieber et al., 2023), which may indicate that these aerosols are of an anthropogenic origin (e.g., Rehkämper et al., 2012). Lateral inputs of dust to low Cd surface waters have caused Cd trends to deviate from the biologically mediated trends toward these lighter values (Sieber et al., 2023), as we observe in the sediment. Additionally, the upward mixing of deep waters may also contribute to the lighter-than-expected δ^{114}Cd in these low [Cd] regions (Abouchami et al., 2011; Xue et al., 2013). This process has been previously documented for multiple regions of the ocean: whereas δ^{114}Cd of surface seawater follows a Rayleigh- or Rayleigh-like trend at high [Cd], this relationship breaks down at very low Cd concentrations (Fig. 10). When plotted together, the dissolved and sedimentary data indicate a positive trend of increasing sedimentary δ^{114}Cd with surface seawater [Cd] until dissolved concentrations reach ≈0.15 nM (Fig. 10). This trend is consistent with the process of additions of isotopically light Cd aerosol particles that subsequently dissolved and/or upward mixing of deep water with lighter isotope values than overlying surface water. However, individual surface seawater samples provide only a snapshot of the upward mixing processes that are variable both geographically and temporally. In contrast, sediment samples average these processes over longer time periods (in our case decades or more depending on sedimentation rates). The relationship between sedimentary δ^{114}Cd and $[Cd]_{surf}$ may suggest that aeolian deposition of isotopically light particles or upward mixing of deeper waters, over decadal time scales, is the dominant control on sedimentary δ^{114}Cd at low surface Cd concentrations.

It is possible that sediments deposited underneath regions with significantly higher Cd surface concentrations (i.e., 0.15–1.2 nM) do follow the seawater trends that suggest Rayleigh fractionation or open-system steady state fractionation in Cd-replete conditions, unlike the Cd isotope compositions underlying Cd depleted surface waters. We can gain insight into the sedimentary isotope composition underlying Cd replete conditions by considering studies characterizing the Cd isotope systematics in surface waters of Cd-replete regions (Abouchami et al., 2011; Xue et al., 2013). These studies illustrate that in surface waters with a Cd concentration greater than 0.15 nM, higher Cd concentrations are negatively correlated with dissolved δ^{114}Cd (Fig. 10). The application of a constant fractionation factor would allow us to predict the Cd isotope composition of sedimentary organic matter in Cd replete regions of the ocean. According to modeling and field studies, an appropriate fractionation factor for a Cd-replete region would likely fall between Δ^{114}Cd = − 0.25 ‰ and − 0.8 ‰ (Xue et al., 2013), with a value of − 0.4 ‰ dominating in the Southern Ocean. Fig. 10 shows the two relationships, the measured values under the low concentration seawater and the theoretical values under Cd-replete conditions, that may set the Cd isotope composition of the sediment: a broad positive trend for

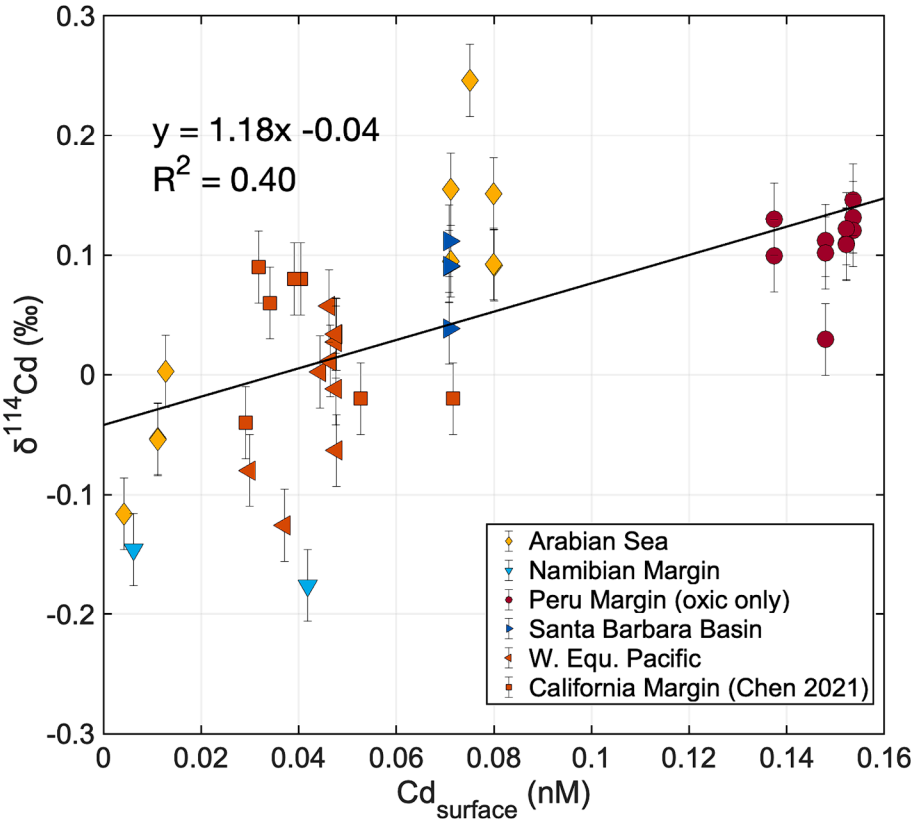

Fig. 9. Sedimentary Cd isotope data plotted against surface-water dissolved [Cd] (dissolved data from Roshan and DeVries, 2021). This correlation suggests that under low surface water Cd concentrations (between 0 and 0.15 nM), the isotope composition becomes lighter as Cd becomes less concentrated in the surface water. This is likely because of the addition of light Cd (via upward mixing of waters or aerosol sources of Cd) becomes relatively more important when the surface Cd concentration is low.

conditions with Cd < 0.15 nM and a negative trend for Cd > 0.15 nM.

5.2.3. Correlations between O_2 and $\delta^{114}Cd$

The second significant correlation is between leachable sedimentary $\delta^{114}Cd$ and bottom-water $[O_2]$. The trend suggests that as bottom water $[O_2]$ increases, the $\delta^{114}Cd$ of sediments becomes lower (Fig. 11). One plausible process likely to govern this trend is Cd isotope fractionation that occurs during organic matter remineralization. To better understand the role that remineralization may play in modifying the $\delta^{114}Cd$ of sinking particles, we examined profiles of $p\delta^{114}Cd$ from the fully oxic water column of the Ross Sea and compared them with $p\delta^{114}Cd$ from OMZs. We compare these two regions as they serve as endmembers of oxygen concentrations in the water column.

The profiles from the Ross Sea were collected in a fully oxic water column ($[O_2] \geq 160$ μM; Fig. 4a-d). In contrast, two other studies in the northeast Pacific and North Atlantic have measured $p\delta^{114}Cd$ in regions with lower oxygen. Samples from Janssen et al., (2019) covered a region with expansive low O_2 subsurface waters, in places reaching O_2 levels as low as ≈10 μM. Janssen et al. (2014) reported $p\delta^{114}Cd$ from the Mauritanian Upwelling zone, a region with subsurface O_2 concentrations that reached a minimum of ≈50 μM. Profiles from the Ross Sea, the northeast Pacific profiles (0.8–51 μm size fraction), and the North Atlantic profiles (>0.2 μm size fraction) all show similar depth-dependent changes in $p\delta^{114}Cd$; surface samples possess heavy values, the subsurface samples trend toward lighter values, and the deepest samples return toward heavier values, although never reaching compositions as heavy as the corresponding surface value. It is worth noting that these profiles cover different depth ranges, with the Ross Sea and North Atlantic data spanning the surface to between 400 and 600 m, while the two Pacific profiles extend to around 1,500 m. Despite the differences, there is substantial and similar vertical variation in $p\delta^{114}Cd$ in both fully oxic water columns and within OMZs. The depth-dependent changes in $p\delta^{114}Cd$ may be due to fractionation during remineralization or preferential remineralization of pools of Cd with variable lability (Bourne et al., 2018; Janssen et al., 2019).

The Cd isotope offset between the large and small size fraction

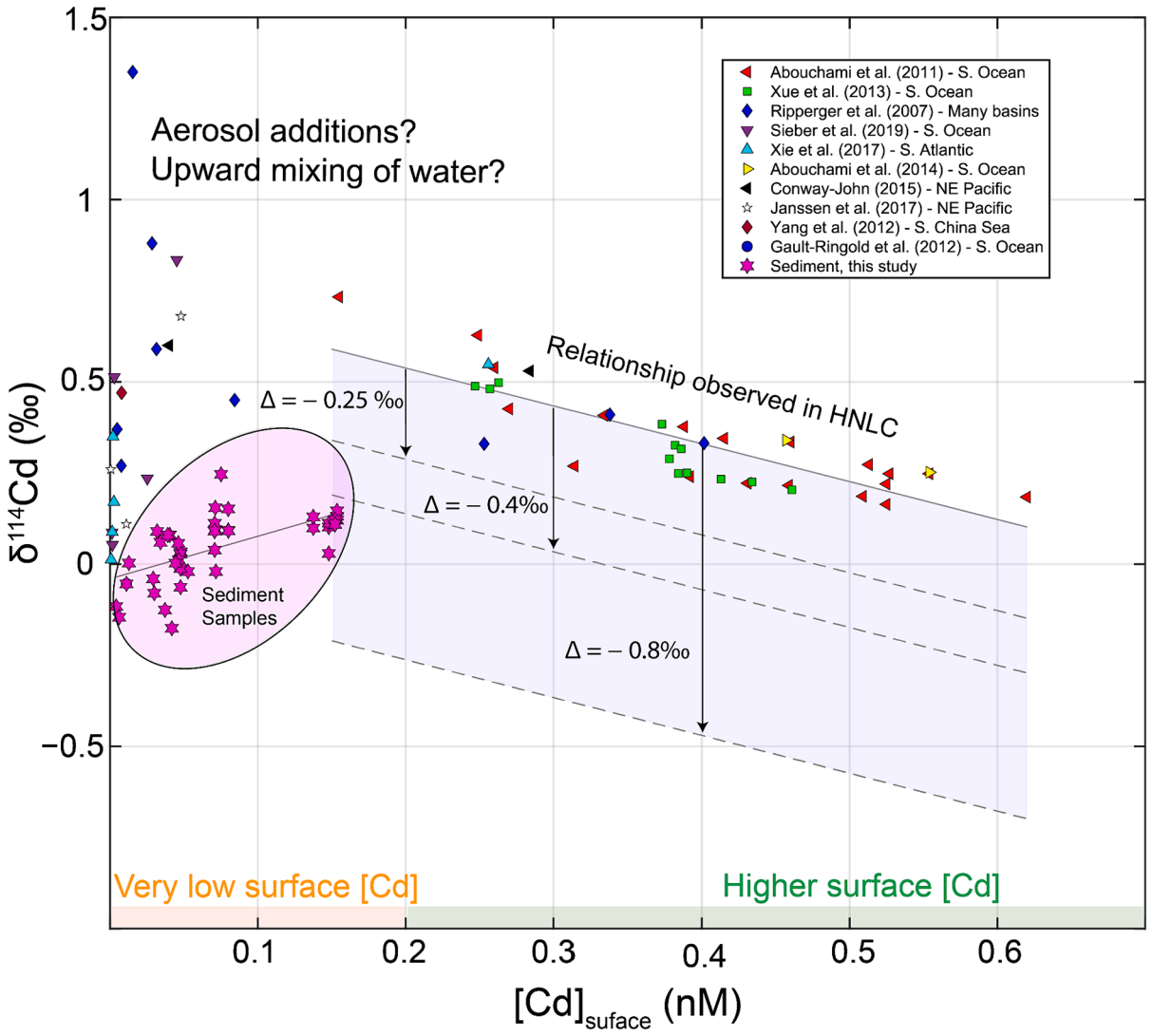

Fig. 10. Cd isotope composition of sediments and seawater against dissolved surface Cd concentrations. Dissolved $\delta^{114}Cd$ surface seawater samples versus surface Cd concentrations are shown alongside $\delta^{114}Cd$ sediment samples (highlighted in pink). The seawater data at [Cd] concentrations < 0.15 nM fall off the expected HNLC Rayleigh fractionation relationship. The pink stars are sediment data from this study and Chen et al. (2021). They show in regions with low surface Cd that the sediment samples are characterized by a broad positive trend. This is likely related to additions from deepwater and aerosols. The shaded purple region is the range of expected sediment values if the seawater rayleigh-like behavior is preserved in the sediment underlying regions with higher surface Cd concentrations. The fractionation factors shown here include $\Delta^{114}Cd = -0.25, -0.4$, or -0.8 ‰. The general location for the seawater samples is given in the legend name and the sediment locations can be seen in Fig. 9.

particles is also noteworthy and points towards differences in the nature of the biogeochemical processing taking place within each size class. Here we briefly consider possible driving processes, including remineralization, secondary particle formation, and dynamical considerations unique to the Ross Sea. Likewise, the small size particles may not accurately represent the particles that ultimately reach the seafloor; small particles sink much more slowly than large particles, if at all, and may undergo more processing before arriving at the seafloor. This is consistent with the observation that profiles of LSF exhibit comparatively smaller depth-dependent variations in $p\delta^{114}Cd$, potentially indicating less Cd isotope modification during transit through the water column. Indeed, all subsurface Ross Sea LSF samples from Stations 0, 2, and 24, are identical, within uncertainty, to all other Cd isotope compositions within the same profile, excepting one subsurface sample at St. 24, (Fig. 4e-h). However, most of the samples in the Ross Sea data were taken on the continental shelf and thus cover only the upper ≈400 m of water depth. Deeper data from Station 14, which was located beyond the shelf break with water depth of 1,887 m, suggests that there may be other processes that modify the $p\delta^{114}Cd$ of large particles deeper in the water column.

Assuming that sinking particles represent the residual material that is not remineralized, our paired data suggest that remineralization tends to concentrate light Cd isotopes in the SSF and render exported LSF material heavy. This finding would implicate heterotrophic processes in setting the $p\delta^{114}Cd$ of suspended and sinking organic matter. It is also possible that the different size classes represent different pools of sinking material, such as microbes and zooplankton, that have different Cd isotope fractionation factors. The differences in Cd and P remineralization point to variable remineralization processes in sinking particles. Fig. 4 (q-t) indicates significant variability in particulate Cd:P in both size classes. Generally, both size classes show increases in Cd:P with depth, reaching a maximum in the mesopelagic, before decreasing toward surface-like values below 400 m. Such patterns may reflect preferential remineralization of P, relative to Cd, in the mid-depths, or a small gain of Cd (relative to P), as organic matter is remineralized. Given that preferential remineralization of P is not expected to induce Cd isotope fractionation, the significant variation in profiles of $p\delta^{114}Cd$ may point towards small gains in isotopically fractionated particulate Cd—particularly in the small size fraction—as being the dominant process.

Seasonality and lateral advection may also influence the Cd isotope composition of the particles. The Ross Sea experiences large seasonal changes due to ice coverage for most of the year and significant phytoplankton blooms in the spring. The large seasonal differences likely lead to variable residence times of small and large particles. While material in the LSF may be dominated by the seasonal bloom, SSF particles may be able to accumulate over several years. Likewise, if the SSF particles sink slowly and can accumulate in the water column, the composition of the particles is likely to be affected by lateral advection. The regional circulation is characterized by advective inputs from the east and exchanges with off-shelf regions to the north (Smith Jr et al., 2014). Bochdansky et al. (2017) analyzed particles between 200 and 300 m of water depth and found that the particles were well correlated with particle abundances in the mixed layer. Thus, the authors of the study concluded that most of the particles near this water depth were supplied by export rather than lateral advection. The majority of our samples come from water depths between 0 and 400 m, and thus likely reflect export processes. Indirect evidence also supports the idea that vertical processes, not advection, drive the evolution of Cd isotopes in the water column. We observe that the Ross Sea, North Pacific, and Tropical Atlantic, wherein the LSF and SSF particle fractions are consistently offset suggest that a relationship between the SSF and LSF is important for controlling Cd isotope compositions. Additional research is needed, ideally focusing on both large- and small-size fraction particles across variations in the subsurface microbial community, redox conditions, and considering both the entirety of the water column and

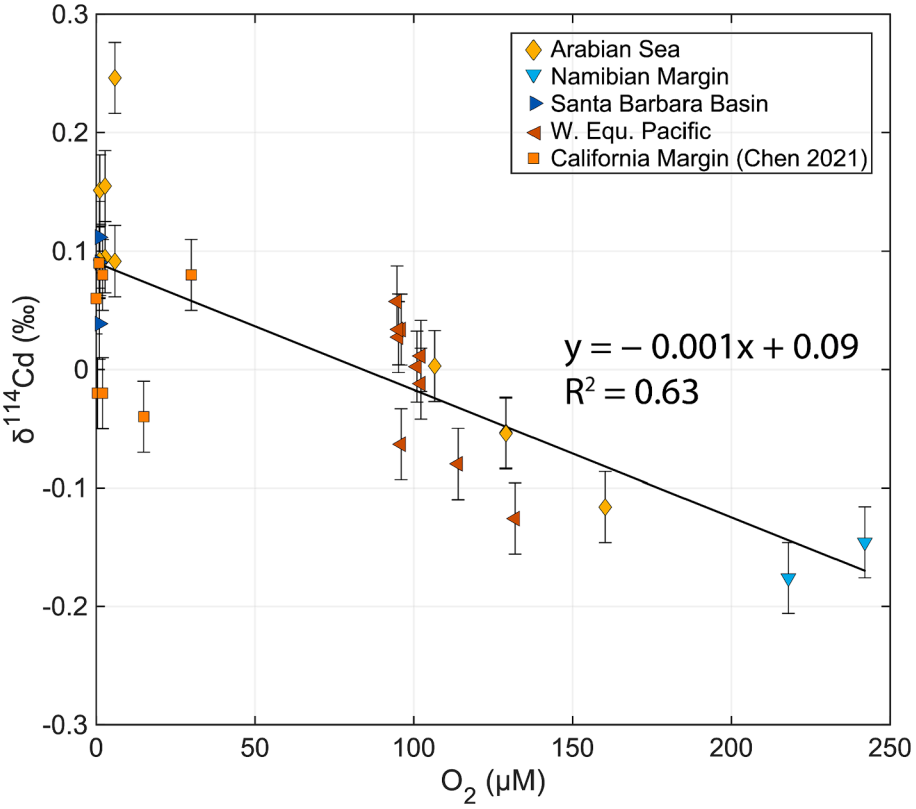

Fig. 11. Sedimentary Cd isotope data against bottom-water [O_2]. Bottom water oxygen value measured or estimated from WOA18, against sediment $\delta^{114}Cd$. All sediments with evidence for CdS influences are removed. Only oxic and suboxic sediments are included in this figure.

lateral advection. Such studies will help to determine the mechanisms affecting particulate Cd isotope fractionation as well as the Cd isotope compositions of organic matter that is ultimately delivered to and incorporated in sediments.

While the particulate data supports a link between remineralization and Cd isotope fractionation, the $p\delta^{114}Cd$ values themselves do not explain the trends observed in the sediments. The suspended SSF particles have light $p\delta^{114}Cd$ regardless of the $[O_2]$ in the water column, as shown by the similar relationships in the oxic Southern Ocean and the OMZ in the Pacific Ocean. In contrast, we observe decreases in sedimentary $\delta^{114}Cd$ with increasing bottom-water $[O_2]$. Currently, there is no clear way to relate the correlation between sedimentary $\delta^{114}Cd$ with the water column particulate profiles. However, despite not having a clear explanation for the link between bottom water oxygen and sedimentary $\delta^{114}Cd$, our sediment data do show a correlation that might be related to some aspect of organic matter remineralization.

6. Conclusions and implications

We considered three driving questions in this research: (i) Can we differentiate between regions that have substantial CdS formation from those that do not, and what are the Cd isotope consequences? (ii) Is there a way to establish a connection between the Cd isotope composition of sinking and suspended particulate matter and observations on the seafloor? And, (iii) Do regions primarily influenced by Cd derived from organic matter reflect nutrient utilization from surface waters?

We first show that we can diagnose regions with significant CdS input by examining Cd content relative to organically derived Cd and the isotope composition of sediment. Sediments with the highest Cd content were found to be associated with significant pelagic CdS formation, geographically connected to upwelled dissolved Cd sources and having a supply of dissolved H_2S. However, these regions with pelagically precipitated CdS have a limited areal extent and thus likely exert only a minor impact on the global Cd budget.

We then investigated the Cd isotope composition of sediments in both oxic and suboxic regions. Our findings reveal that almost all sediments exhibit light Cd isotope compositions, not just those within OMZs. Moreover, we find that more oxic bottom waters are generally associated with lighter sedimentary Cd isotope compositions. In contrast, profiles of marine particulate matter showed that large particles, most likely to reach the seafloor, became increasingly heavy during export. Additionally, we observed that sedimentary Cd isotope compositions were positively correlated with surface-water [Cd], attributed to upward mixing of deeper waters or downward inputs from aerosols. However, we note a general absence of sediments underlying Cd-replete regions, where sedimentary Cd isotope compositions are expected to follow biologically driven fractionation trends. Future studies are encouraged to analyze samples from these regions to determine whether sediments can record the observed fractionation in surface waters.

Our data show that there is no single variable that can predict the Cd isotope composition of marine sediments. Instead, we show that sedimentary Cd isotope systematics are correlated with multiple properties, such as bottom-water $[O_2]$ and surface-water [Cd], which are controlled by different processes. This complexity in teasing out a unique driving process introduces uncertainty when relating sedimentary Cd isotopes to nutrient utilization and in establishing the global mass balance of Cd isotopes. Should the relationships with surface-water [Cd] and bottom-water $[O_2]$ be subsequently refined, sedimentary Cd isotopes may still offer valuable insights as a biogeochemical proxy for these properties.

Data availability

Data are available through Mendeley Data at https://doi.org/10.17632/8smwrc7dgz.1.

CRediT authorship contribution statement

Logan A. Tegler: Writing – review & editing, Writing – original draft, Visualization, Validation, Software, Resources, Methodology, Investigation, Funding acquisition, Formal analysis, Data curation, Conceptualization. **Sune G. Nielsen:** Writing – review & editing, Writing – original draft, Visualization, Validation, Supervision, Software, Resources, Project administration, Methodology, Investigation, Funding acquisition, Formal analysis, Data curation, Conceptualization. **Yi Wang:** Writing – review & editing, Validation, Software, Resources. **Florian Scholz:** Writing – review & editing, Validation, Resources. **Jeremy D. Owens:** Writing – review & editing, Validation, Resources. **Larry Peterson:** Writing – review & editing, Validation, Resources. **Maureen Auro:** Writing – review & editing, Resources, Methodology, Formal analysis. **Christopher W. Kinsley:** Investigation, Conceptualization. **Phoebe Lam:** Writing – review & editing, Validation, Resources. **Tristan J. Horner:** Writing – review & editing, Writing – original draft, Visualization, Validation, Supervision, Software, Resources, Project administration, Methodology, Investigation, Funding acquisition, Formal analysis, Data curation, Conceptualization.

Declaration of competing interest

The authors declare that they have no known competing financial interests or personal relationships that could have appeared to influence the work reported in this paper.

Acknowledgments

We would like to acknowledge Jurek Blusztajn for his invaluable help running the MC-ICP-MS at WHOI. The project was funded by the National Science Foundation Graduate Research Fellowship (Grant #1122374; L.A.T). TJH also acknowledges support from NSF (OCE-1443577 and OCE-2023456) and *The Breene M. Kerr Early Career Scientist Endowment Fund.*

Appendix A. Supplementary material

Supplementary data can be found in Tables S1 (leaching test geochemical data), S2 (auxiliary data for each sediment sample), and S3 (coefficients for the multiple linear regression).

Supplementary material to this article can be found online at https://doi.org/10.1016/j.gca.2024.03.010.

References

Abouchami, W., Galer, S.J.G., De Baar, H.J.W., Alderkamp, A.C., Middag, R., Laan, P., Feldmann, H., Andreae, M.O., 2011. Modulation of the Southern Ocean cadmium isotope signature by ocean circulation and primary productivity. Earth Planet Sc. Lett. 305 (1–2), 83–91.

Abouchami, W., Galer, S.J., Horner, T.J., Rehkämper, M., Wombacher, F., Xue, Z., Lambelet, M., Gault-Ringold, M., Stirling, C.H., Schönbächler, M., Shiel, A.E., Weis, D., Holdship, P.F., 2013. A common reference material for cadmium isotope studies–NIST SRM 3108. Geostand. Geoanal. Res. 37, 5–17.

Abouchami, W., Galer, S.J.G., De Baar, H.J.W., Middag, R., Vance, D., Zhao, Y., Feldmann, H., Andreae, M.O., 2014. Biogeochemical cycling of cadmium isotopes in the Southern Ocean along the Zero Meridian. Geochim. Cosmochim. Ac 127, 348–367.

Arthur, M.A., Dean, W.E., Neff, E.D., Hay, B.J., King, J., Jones, G., 1994. Varve calibrated records of carbonate and organic carbon accumulation over the last 2000 years in the Black Sea. Global Biogeochem Cy 8, 195–217.

Astor Y. M., Lorenzoni L. and Scranton M. 2011. Handbook of methods for the analysis of oceanographic parameters at the Cariaco time series station. Available on line at: https://repository.oceanbestpractices.org/.

Bernhard, J.M., Reimers, C.E., 1991. Benthic foraminiferal population fluctuations related to anoxia: Santa Barbara Basin. Biogeochemistry 15, 127–149.

Bernhard, J.M., Sen Gupta, B.K., Borne, P.F., 1997. Benthic foraminiferal proxy to estimate dysoxic bottom-water oxygen concentrations; Santa Barbara Basin, US Pacific continental margin. J. Foramin. Res. 27 (4), 301–310.

Bishop, J.K., Lam, P.J., Wood, T.J., 2012. Getting good particles: Accurate sampling of particles by large volume in-situ filtration. Limnology Oceanogr. Methods 10 (9), 681–710.

Bishop, J.K., Wood, T.J., 2008. Particulate matter chemistry and dynamics in the twilight zone at VERTIGO ALOHA and K2 sites. Deep Sea Res. Part : Oceanogr. Res. Pap. 55 (12), 1684–1706.
Bochdansky, A.B., Clouse, M.A., Hansell, D.A., 2017. Mesoscale and high-frequency variability of macroscopic particles (> 100 μm) in the Ross Sea and its relevance for late-season particulate carbon export. J. Mar. Syst. 166, 120–131.
Bourne, H.L., Bishop, J.K., Lam, P.J., Ohnemus, D.C., 2018. Global spatial and temporal variation of Cd: P in euphotic zone particulates. Global Biogeochem. Cy. 32, 1123–1141.
Boyer, Garcia T. P. , Locarnini H. E. , Zweng R. A. , Mishonov M. M. , Reagan A. V. , Weathers J. R., Baranova K. A. , Seidov O. K. , Smolyar D. and V. I. 2022. World Ocean Atlas 2018. NOAA National Centers for Environmental Information. Dataset.
Boyle, E.A., 1988. Cadmium: Chemical tracer of deepwater paleoceanography. Paleoceanography 3, 471–489.
Boyle, E.A., Sclater, F., Edmond, J., 1976. On the marine geochemistry of cadmium. Nature 263, 42–44.
Bridgestock, L., Rehkämper, M., Van De Flierdt, T., Murphy, K., Khondoker, R., Baker, A. R., et al., 2017. The Cd isotope composition of atmospheric aerosols from the Tropical Atlantic Ocean. Geophys Res. Lett. 44, 2932–2940.
Brüchert, V., Currie, B., Peard, K. R., Lass, U., Endler, R., Dübecke, A., et al.. 2006. Shelf anoxia in the Namibian coastal upwelling system. Biogeochemical and physical control on shelf anoxia and water column hydrogen sulphide in the Benguela coastal upwelling system off Namibia. Past and present water column anoxia. NATO Science Series. Kluwer Springer, 161-193.
Bruland, K.W., 1980. Oceanographic distributions of cadmium, zinc, nickel, and copper in the North Pacific. Earth Planet Sc. Lett. 47, 176–198.
Bryan, A.L., Dickson, A.J., Dowdall, F., Homoky, W.B., Porcelli, D., Henderson, G.M., 2021. Controls on the cadmium isotope composition of modern marine sediments. Earth Planet Sc. Lett. 565, 116946.
Chapman, P., Shannon, L.V., 1987. Seasonality in the oxygen minimum layers at the extremities of the Benguela system. South Afr. J. Mar. Sci. 5, 85–94.
Chen, L., Little, S.H., Kreissig, K., Severmann, S., McManus, J., 2021. Isotopically light Cd in sediments underlying oxygen deficient zones. Frontiers Earth Sci. 9, 623720.
Conway, T.M., John, S.G., 2015a. Biogeochemical cycling of cadmium isotopes along a high-resolution section through the North Atlantic Ocean. Geochim. Cosmochim. Ac 148, 269–283.
Conway, T.M., John, S.G., 2015b. The cycling of iron, zinc and cadmium in the North East Pacific Ocean-Insights from stable isotopes. Geochim. Cosmochim. Ac 164, 262–283.
Conway, T.M., Rosenberg, A.D., Adkins, J.F., John, S.G., 2013. A new method for precise determination of iron, zinc and cadmium stable isotope ratios in seawater by double-spike mass spectrometry. Anal. Chim. Acta 793, 44–52.
Currie, B., Utne-Palm, A.C., Salvanes, A.G.V., 2018. Winning ways with hydrogen sulphide on the Namibian shelf. Front. Mar. Sci. 5, 341.
Cutter, G., Andersson, P., Codispoti, L., Croot, P., Francois, R., Lohan, M. C., et al., 2010. Sampling and sample-handling protocols for GEOTRACES cruises.
Dale, A.W., Sommer, S., Lomnitz, U., Montes, I., Treude, T., Liebetrau, V., et al., 2015. Organic carbon production, mineralisation and preservation on the Peruvian margin. Biogeosciences 12, 1537–1559.
Dale, A.W., Paul, K.M., Clemens, D., Scholz, F., Schroller-Lomnitz, U., Wallmann, K., et al., 2021. Recycling and burial of biogenic silica in an open margin oxygen minimum zone. Global Biogeochem. Cy. 35, e2020GB006583.
Davies-Colley, R.J., Nelson, P.O., Williamson, K.J., 1985. Sulfide control of cadmium and copper concentrations in anaerobic estuarine sediments. Mar. Chem. 16, 173–186.
de Souza, G.F., Vance, D., Sieber, M., Conway, T.M., Little, S.H., 2022. Re-assessing the influence of particle-hosted sulphide precipitation on the marine cadmium cycle. Geochim. Cosmochim. Ac 322, 274–296.
Farmer, J. R., Hertzberg, J. E., Cardinal, D., Fietz, S., Hendry, K., Jaccard, S. L., et al. GEOTRACESPAGES Biological Productivity Working Group Members. 2021. Assessment of C, N, and Si isotopes as tracers of past ocean nutrient and carbon cycling.
Gault-Ringold, M., Adu, T., Stirling, C.H., Frew, R.D., Hunter, K.A., 2012. Anomalous biogeochemical behavior of cadmium in subantarctic surface waters: mechanistic constraints from cadmium isotopes. Earth Planet Sc. Lett. 341, 94–103.
George, E., Stirling, C.H., Gault-Ringold, M., Ellwood, M.J., Middag, R., 2019. Marine biogeochemical cycling of cadmium and cadmium isotopes in the extreme nutrient-depleted subtropical gyre of the South West Pacific Ocean. Earth Planet Sc. Lett. 514, 84–95.
Georgiev, S.V., Horner, T.J., Stein, H.J., Hannah, J.L., Bingen, B., Rehkämper, M., 2015. Cadmium-isotopic evidence for increasing primary productivity during the Late Permian anoxic event. Earth Planet Sc. Lett. 410, 84–96.
Gobeil, C., Silverberg, N., Sundby, B., Cossa, D., 1987. Cadmium diagenesis in Laurentian Trough sediments. Geochim. Cosmochim. Ac 51, 589–596.
Guinoiseau, D., Galer, S.J., Abouchami, W., 2018. Effect of cadmium sulphide precipitation on the partitioning of Cd isotopes: Implications for the oceanic Cd cycle. Earth Planet Sc. Lett. 498, 300–308.
Ho, T.Y., Quigg, A., Finkel, Z.V., Milligan, A.J., Wyman, K., Falkowski, P.G., Morel, F.M., 2003. The elemental composition of some marine phytoplankton. J. Phycol 39, 1145–1159.
Hohl, S.V., Jiang, S.Y., Wei, H.Z., Pi, D.H., Liu, Q., Viehmann, S., Galer, S.J., 2019. Cd isotopes trace periodic (bio) geochemical metal cycling at the verge of the Cambrian animal evolution. Geochim. Cosmochim. Ac 263, 195–214.
Horner, T.J., Schönbächler, M., Rehkämper, M., Nielsen, S.G., Williams, H., Halliday, A. N., Xue, Z., Hein, J.R., 2010. Ferromanganese crusts as archives of deep water Cd isotope compositions. Geochem Geophys Geosystems 11.
Horner, T.J., Rickaby, R.E., Henderson, G.M., 2011. Isotopic fractionation of cadmium into calcite. Earth Planet Sc. Lett. 312, 243–253.
Horner, T.J., Lee, R.B., Henderson, G.M., Rickaby, R.E., 2013. Nonspecific uptake and homeostasis drive the oceanic cadmium cycle. Proc. National Acad. Sci. 110, 2500–2505.
Horner, T.J., Pryer, H.V., Nielsen, S.G., Crockford, P.W., Gauglitz, J.M., Wing, B.A., Ricketts, R.D., 2017. Pelagic barite precipitation at micromolar ambient sulfate. Nat. Commun. 8, 1342.
Horner, T.J., Little, S.H., Conway, T.M., Farmer, J.R., Hertzberg, J.E., Janssen, D.J., Lough, A.J.M., McKay, J.L., Tessin, A., Galer, S.J.G., Jaccard, S.L., Lacan, F., Paytan, A., Wuttig, K., 2021. Bioactive Trace Metals and Their Isotopes as Paleoproductivity Proxies: An Assessment Using GEOTRACES-Era Data. Global Biogeochem. Cycles 35, 1–86.
Jahnke, R. A. 2010. "Global synthesis". In: Liu, K., Atkinson, L., Quiñones, R. and Talaue-McManus, L. (Eds.), Carbon and nutrient fluxes in continental margins. Global change—the IGBP series. Berlin: Springer. https://doi.org/10.1007/978-3-540-92735-8.
Janssen, D.J., Conway, T.M., John, S.G., Christian, J.R., Kramer, D.I., Pedersen, T.F., Cullen, J.T., 2014. Undocumented water column sink for cadmium in open ocean oxygen-deficient zones. Proc. National Acad. Sci. 111, 6888–6893.
Janssen, D.J., Abouchami, W., Galer, S.J., Purdon, K.B., Cullen, J.T., 2019. Particulate cadmium stable isotopes in the subarctic northeast Pacific reveal dynamic Cd cycling and a new isotopically light Cd sink. Earth Planet Sc. Lett. 515, 67–78.
Jochum, K.P., Nohl, U., Herwig, K., Lammel, E., Stoll, B., Hofmann, A.W., 2005. GeoReM: a new geochemical database for reference materials and isotopic standards. Geostand. Geoanal. Res. 29, 333–338.
John, S.G., Conway, T.M., 2014. A role for scavenging in the marine biogeochemical cycling of zinc and zinc isotopes. Earth Planet Sc. Lett. 394, 159–167.
John, S.G., Helgoe, J., Townsend, E., 2018. Biogeochemical cycling of Zn and Cd and their stable isotopes in the Eastern Tropical South Pacific. Mar. Chem. 201, 256–262.
Konovalov, S.K., Ivanov, L.I., Samodurov, A.S., 2001. Fluxes and budget of sulphide and ammonia in the Black Sea anoxic layer. J. Marine Syst. 31, 203–216.
Konovalov, S.K., Murray, J.W., 2001. Variations in the chemistry of the Black Sea on a time scale of decades (1960–1995). J. Marine Syst. 31, 217–243.
Lacan, F., Francois, R., Ji, Y., Sherrell, R.M., 2006. Cadmium isotopic composition in the ocean. Geochim. Cosmochim. Ac 70, 5104–5118.
Lambelet, M., Rehkämper, M., van de Flierdt, T., Xue, Z., Kreissig, K., Coles, B., et al., 2013. Isotopic analysis of Cd in the mixing zone of Siberian rivers with the Arctic Ocean—New constraints on marine Cd cycling and the isotope composition of riverine Cd. Earth Planet Sc. Lett. 361, 64–73.
Lane, T.W., Saito, M.A., George, G.N., Pickering, I.J., Prince, R.C., Morel, F.M., 2005. A cadmium enzyme from a marine diatom. Nature 435, 42.
Little, S.H., Vance, D., Lyons, T.W., McManus, J., 2015. Controls on trace metal authigenic enrichment in reducing sediments: insights from modern oxygen-deficient settings. Am. J. Sci. 315, 77–119.
Lu, Z., Zhu, J.M., Tan, D., Wang, X., Zheng, Z., 2021. δ114/110Cd values of a suite of different reference materials. Geostand. Geoanal. Res. 45, 565–581.
Marchitto, T.M., Broecker, W.S., 2006. Deep water mass geometry in the glacial Atlantic Ocean: A review of constraints from the paleonutrient proxy Cd/Ca. Geochem., Geophys., Geosystems 7.
McCorkle, D.C., Klinkhammer, G.P., 1991. Porewater cadmium geochemistry and the porewater cadmium: δ13C relationship. Geochim. Cosmochim. Ac 55, 161–168.
McManus, J., Berelson, W.M., Coale, K.H., 1997. Phosphorus regeneration in continental margin sediments. Oceanogr. Lit. Rev. 1, 61.
Moore, C.M., Mills, M.M., Arrigo, K.R., Berman-Frank, I., Bopp, L., Boyd, P.W., et al., 2013. Processes and patterns of oceanic nutrient limitation. Nat. Geosci. 6, 701–710.
Morford, J.L., Emerson, S., 1999. The geochemistry of redox sensitive trace metals in sediments. Geochim. Cosmochim. Ac 63, 1735–1750.
Murphy, K., Rehkämper, M., Kreissig, K., Coles, B., van de Flierdt, T., 2016. Improvements in Cd stable isotope analysis achieved through use of liquid–liquid extraction to remove organic residues from Cd separates obtained by extraction chromatography. J. Anal. Atom. Spectrom. 31, 319–327.
Nielsen, S.G., Goff, M., Hesselbo, S.P., Jenkyns, H.C., LaRowe, D.E., Lee, C.T.A., 2011. Thallium isotopes in early diagenetic pyrite–A paleoredox proxy? Geochim. Cosmochim. Ac 75, 6690–6704.
Ohde, T., 2018. Coastal sulfur plumes off Peru during El Niño, La Niña, and neutral phases. Geophys Res. Lett. 45, 7075–7083.
Ohnemus, D.C., Rauschenberg, S., Cutter, G.A., Fitzsimmons, J.N., Sherrell, R.M., Twining, B.S., 2017. Elevated trace metal content of prokaryotic communities associated with marine oxygen deficient zones. Limnol. Oceanogr. 62, 3–25.
Ostrander, C.M., Owens, J.D., Nielsen, S.G., 2017. Constraining the rate of oceanic deoxygenation leading up to a Cretaceous Oceanic Anoxic Event (OAE-2:≈ 94 Ma). Sci. Advances 3, e1701020.
Owens, J.D., Nielsen, S.G., Horner, T.J., Ostrander, C.M., Peterson, L.C., 2017. Thallium-isotopic compositions of euxinic sediments as a proxy for global manganese-oxide burial. Geochim. Cosmochim. Ac 213, 291–307.
Pennington, J.T., Mahoney, K.L., Kuwahara, V.S., Kolber, D.D., Calienes, R., Chavez, F.P., 2006. Primary production in the eastern tropical Pacific: A review. Prog. Oceanogr.y 69, 285–317.
Peterson, L. C., Overpeck, J. T., & Murray, D. W. 1990. A High-Resolution Paleoenvironmental Study of the Cariaco Basin, Venezuela: Late Quaternary to Present-Preliminary Report on R/V Thomas Washington Cruise PLUME-07. RSMAS/University of Miami Technical Report, 50.
Planquette, H., Sherrell, R.M., 2012. Sampling for particulate trace element determination using water sampling bottles: methodology and comparison to in situ pumps. Limnology Oceanogr. Methods 10, 367–388.

Plass, A., Schlosser, C., Sommer, S., Dale, A.W., Achterberg, E.P., Scholz, F., 2020. The control of hydrogen sulfide on benthic iron and cadmium fluxes in the oxygen minimum zone off Peru. Biogeosciences 17, 3685–3704.
Plass, A., Dale, A.W., Scholz, F., 2021. Sedimentary cycling and benthic fluxes of manganese, cobalt, nickel, copper, zinc and cadmium in the Peruvian oxygen minimum zone. Mar. Chem. 233, 103982.
Rehkämper, M., Wombacher, F., Horner, T.J., Xue, Z., 2012. Natural and anthropogenic Cd isotope variations. Handbook of Environmental Isotope Geochemistry: Vol I, 125–154.
Ripperger, S., Rehkämper, M., Porcelli, D., Halliday, A.N., 2007. Cadmium isotope fractionation in seawater—A signature of biological activity. Earth Planet Sc. Lett. 261, 670–684.
Rosenthal, Y., Lam, P., Boyle, E.A., Thomson, J., 1995a. Authigenic cadmium enrichments in suboxic sediments: Precipitation and postdepositional mobility. Earth Planet Sc. Lett. 132, 99–111.
Rosenthal, Y., Boyle, E.A., Labeyrie, L., Oppo, D., 1995b. Glacial enrichments of authigenic Cd and U in Subantarctic sediments: A climatic control on the elements' oceanic budget? Paleoceanography 10, 395–413.
Roshan, S., DeVries, T., 2021. Global contrasts between oceanic cycling of cadmium and phosphate. Global Biogeochem. Cy. 35, e2021GB006952.
Schlitzer, R. 2017. Ocean data view. Retrieved from http.*odv.awi.de*.
Schmitt, A.D., Galer, S.J., Abouchami, W., 2009. Mass-dependent cadmium isotopic variations in nature with emphasis on the marine environment. Earth Planet Sc. Lett. 277, 262–272.
Scholz, F., Hensen, C., Noffke, A., Rohde, A., Liebetrau, V., Wallmann, K., 2011. Early diagenesis of redox-sensitive trace metals in the Peru upwelling area–response to ENSO-related oxygen fluctuations in the water column. Geochim. Cosmochim. Ac 75, 7257–7276.
Scholz, F., Löscher, C.R., Fiskal, A., Sommer, S., Hensen, C., Lomnitz, U., et al., 2016. Nitrate-dependent iron oxidation limits iron transport in anoxic ocean regions. Earth Planet Sc. Lett. 454, 272–281.
Schunck, H., Lavik, G., Desai, D.K., Großkopf, T., Kalvelage, T., Löscher, C.R., et al., 2013. Giant hydrogen sulfide plume in the oxygen minimum zone off Peru supports chemolithoautotrophy. PLoS One 8, e68661.
Shannon L. V. and Nelson G. (1996) The Benguela: large scale features and processes and system variability. In The south atlantic. In *The South Atlantic* pp. 163–210.
Sieber, M., Lanning, N.T., Bunnell, Z.B., Bian, X., Yang, S.C., Marsay, C.M., et al., 2023. Biological, physical, and atmospheric controls on the distribution of cadmium and its isotopes in the Pacific Ocean. Global Biogeochem. Cy. 37, e2022GB007441.
Sommer, S., Gier, J., Treude, T., Lomnitz, U., Dengler, M., Cardich, J., Dale, A.W., 2016. Depletion of oxygen, nitrate and nitrite in the Peruvian oxygen minimum zone cause an imbalance of benthic nitrogen fluxes. Deep Sea Res. Part : Oceanogr. Res. Pap. 112, 113–122.
Suess, E., von Huene, R., 1988. Ocean Drilling Program Leg 112, Peru continental margin: Part 2, Sedimentary history and diagenesis in a coastal upwelling environment. Geology 16, 939–943.
Sunda, W.G., 2012. Feedback interactions between trace metal nutrients and phytoplankton in the ocean. Front. Microbiol. 3, 204.
Tankéré, S.P.C., Muller, F.L.L., Burton, J.D., Statham, P.J., Guieu, C., Martin, J.M., 2001. Trace metal distributions in shelf waters of the northwestern Black Sea. Cont. Shelf Res. 21, 1501–1532.
Taylor, J. R. 1982. An introduction to error analysis: the study of uncertainties in physical measurements. ed. Ann, Univ. Sci. Books, Mill Valley, California.
Thunell, R.C., Tappa, E., Anderson, D.M., 1995. Sediment fluxes and varve formation in Santa Barbara Basin, offshore California. Geology 23, 1083–1086.
van Aken, H.M., Verbeek, H., 1988. The hydrography and ventilation of Kau Bay in Halmahera. Neth. J. Sea Res. 22, 403–413.
van der Weijden, C.H., de Lange, G.J., Middelburg, J.J., van der Sloot, H.A., Hoede, D., Shofiyah, S., 1989. Geochemical characteristics of Kau Bay water. Neth. J. Sea Res. 24, 583–589.
van Geen, A., McCorkle, D.C., Klinkhammer, G.P., 1995. Sensitivity of the phosphate-cadmium-carbon isotope relation in the ocean to cadmium removal by suboxic sediments. Paleoceanography 10, 159–169.
Wedepohl, K.H., 1995. The composition of the continental crust. Geochim. Cosmochim. Ac 59, 1217–1232.
Wombacher, F., Rehkämper, M., Mezger, K., Münker, C., 2003. Stable isotope compositions of cadmium in geological materials and meteorites determined by multiple-collector ICPMS. Geochim. Cosmochim. Ac 67, 4639–4654.
Wu, F., Owens, J.D., Scholz, F., Huang, L., Li, S., Riedinger, N., et al., 2020. Sedimentary vanadium isotope signatures in low oxygen marine conditions. Geochim. Cosmochim. Ac 284, 134–155.
Xie, R.C., Galer, S.J., Abouchami, W., Rijkenberg, M.J., De Baar, H.J., De Jong, J., Andreae, M.O., 2017. Non-Rayleigh control of upper-ocean Cd isotope fractionation in the western South Atlantic. Earth Planet Sc. Lett. 471, 94–103.
Xie, R.C., Rehkämper, M., Grasse, P., van de Flierdt, T., Frank, M., Xue, Z., 2019. Isotopic evidence for complex biogeochemical cycling of Cd in the eastern tropical South Pacific. Earth Planet Sc. Lett. 512, 134–146.
Xue, Z., Rehkämper, M., Horner, T.J., Abouchami, W., Middag, R., van de Flierd, T., de Baar, H.J., 2013. Cadmium isotope variations in the Southern Ocean. Earth Planet Sc. Lett. 382, 161–172.
Yakushev, E., Chelysheva, M., Podymov, O., Velikova, V., Chasovnikov, V., Belokopytov, V., 2010. On the recent decadal changes of the Black Sea nutrient regime and oxic/anoxic boundary position. CIESM 25–34.
Yang, S.C., Lee, D.C., Ho, T.Y., 2012. The isotopic composition of cadmium in the water column of the South China Sea. Geochim. Cosmochim. Ac 98, 66–77.
Zhang, Y., Planavsky, N.J., Zhao, M., Isson, T., Asael, D., Wang, C., Wang, F., 2021. The isotopic composition of sedimentary organic zinc and implications for the global Zn isotope mass balance. Geochim. Cosmochim. Acta 314, 16–26.
Zheng, Y., Anderson, R.F., Van Geen, A., Kuwabara, J., 2000. Authigenic molybdenum formation in marine sediments: a link to pore water sulfide in the Santa Barbara Basin. Geochim. Cosmochim. Ac 64, 4165–4178.